Ocean Engineering 260 (2022) 111801

Contents lists available at ScienceDirect

Ocean Engineering

journal homepage: www.elsevier.com/locate/oceaneng

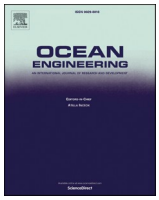

Assessment of allowable sea states for offshore wind turbine blade installation using time-domain numerical models and considering weather forecast uncertainty

Mengning Wu [a,b,*], Zhen Gao [a,c,d], Yuna Zhao [e]

[a] Department of Marine Technology, Norwegian University of Science and Technology (NTNU), Trondheim, 7491, Norway
[b] Bohai Oil Field Research Institute, Tianjin Branch of CNOOC Ltd., Tianjin, 300452, China
[c] Centre for Autonomous Marine Operations and Systems (AMOS), NTNU, Trondheim, 7491, Norway
[d] Centre for Marine Operations in Virtual Environments (MOVE), NTNU, Trondheim, 7491, Norway
[e] Aker Offshore Wind, Oksenøyveien 8, Oslo, 1325, Norway

ARTICLE INFO

Keywords:
Offshore wind turbine
Blade installation
Weather forecasting
Forecast uncertainty quantification
Allowable sea states assessment

ABSTRACT

Installation of offshore wind turbines, particularly blades, is challenging and should be executed within the allowable limit of sea states to ensure the safety and the efficiency of installation. During the execution phase where weather forecast will be used in the decision-making process, uncertainty in weather forecast is an important issue required to be dealt with. The purpose of this paper is to assess allowable sea states for offshore blade installation, with emphasis on both considering weather forecast uncertainty and using time-domain numerical models for installation response analysis. The general procedure is presented, which includes generation of the response-based alpha-factor α_R (that is a reduction indicator reflecting weather forecast uncertainty) in the planning phase based on time-domain modelling and analysis of blade installation, and assessment of corresponding allowable sea states in the execution phase. Single blade installation by a semi-submersible crane vessel at the North Sea center is studied in this paper, and two typical limiting response parameters, namely the blade root radial motion and velocity, are considered. The α_R factors correspond to these two limiting parameters are first generated respectively, based on the forecast uncertainty quantification of sea states, the quantitative assessment of system dynamic responses and the estimation of their characteristic values through probabilistic analysis. The characteristic values of the responses that correspond to a certain exceedance probability (10^{-2} or 10^{-4}) could be generated with and without the consideration of the weather forecast uncertainty. Finally, the allowable sea states with and without the weather forecast uncertainty are obtained when the characteristic value reaches the allowable response limit. These could be further used to identify overall workable weather windows for the offshore blade installation and support operation decision-making. Results indicate that there is a significant difference between the allowable sea states with and without considering weather forecast uncertainty. As the forecast lead time increases, the allowable sea states gradually decrease. Hence, it is necessary to apply α_R to involve and quantify the effect of weather forecast uncertainties on operations. Moreover, since time-domain simulations are used for dynamic response analysis of the installation system, the effect of statistical uncertainty related to the use of a limited number of simulations to derive the characteristic response values is also investigated and is found small.

1. Introduction

Due to the growing interest and demand for clean energy, offshore wind energy as one of the clean, renewable and reliable energy sources, has experienced a rapid development in last decades. Correspondingly, increasing attention has been paid on marine operations associated with the installation of different components (such as foundations, tower, nacelle and blades) of offshore wind turbines (OWTs). Among them, wind turbine blade installation is very challenging due to the high installation precision requirement. Specifically, the large lifting height

* Corresponding author. Department of Marine Technology, Norwegian University of Science and Technology (NTNU), Trondheim, 7491, Norway.
E-mail address: mengning.wu@ntnu.no (M. Wu).

https://doi.org/10.1016/j.oceaneng.2022.111801
Received 1 June 2021; Received in revised form 3 May 2022; Accepted 17 June 2022
Available online 1 August 2022

makes the operation more weather sensitive, and both wave and wind conditions are extremely important for the successful installation.

To date, jack-up crane vessels are commonly used to install the blade of OWTs. They can set legs down to the seabed and then elevate the hull above the sea surface to reduce the impact of waves. Hence, one obvious advantage is that a stable working platform is provided for operations like lifting and mating. Several researchers have focused on marine operations using jack-up vessels and studied their operational limit. For instance, Smith et al. (1996) studied the allowable impact velocities for a jack-up vessel during the standard leg lowering procedure. Thomsen (2014) demonstrated that the jack-up leg lowering and retrieval process are weather-sensitive and the allowable limit for significant wave height H_s is between 1.2 and 1.5 m. Zhao (2019) studied the offshore single blade installation by a jack-up crane vessel and summarized typical operational environmental conditions for the installation, that is, mean wind speed U_w less than 20 m/s and H_s lower than 1.5–2.0 m. Small workable water depth and the large time consumption of the lowering and retrieval processes of jack-up legs are main drawbacks limiting the usage of jack-up crane vessels. In this case, floating crane vessels such as the semi-submersible could be regarded as alternatives. Compared to jack-up crane vessels, floating crane vessels can be located and relocated easier and faster during the installation process. Moreover, due to the wider range of applicable water depths, they have greater flexibility in marine operations. Nevertheless, the blade installation of OWTs by floating crane vessels is not easy since the system is quite sensitive to weather conditions. On one hand, wave-induced motions of the floating crane vessel are relatively larger than that of the jack-up vessel. On the other hand, wind loads on the blade are significant at such a high installation position. Besides, it is expensive to wait for suitable weather on site when using a floating crane vessel. To ensure the safety and cost-efficiency of offshore blade installation, a detailed numerical modelling of such operations is required to assess dynamic responses of the actual installation process. Depending on the operation properties, frequency domain (FD) or time domain (TD) method can be applied. In general, many of the marine operations might be considered using linear potential flow theory for hydrodynamics and linear structural dynamics for rigid-body motion analysis since the operations are often carried out in small or moderate sea conditions. In such cases, it is suitable to study the dynamic response in frequency domain to significantly reduce computational cost. Whereas for complex systems which may involve nonlinear mechanics of the coupling devices or the nonstationary hydrodynamics or structural dynamics due to operational procedures, time domain response analysis approach is more suitable. At present, the time domain response analysis approach is widely used to study dynamic responses of operations with floating systems (Hassan and Soares, 2020; Hudson, 2020; Li et al., 2020; Zhu et al., 2017). For offshore blade installation, many efforts have been made by applying the time domain method to investigate the application potential of using floating crane vessels. For example, Verma et al., 2017, 2019c performed time domain simulations for the blade lifting operation using a floating crane vessel and proposed an approach to estimate limiting sea states. Based on the approach, they conducted damage assessment to investigate the impact behavior of a blade during the lifting process (Verma et al., 2019b). In addition, Zhao et al. (2018a) developed an integrated dynamic analysis method to simulate single blade installation using time-domain numerical models, and proved the feasibility of using a semi-submersible crane vessel for single blade installation, by comparing its performance with a typical jack-up crane vessel (Zhao et al., 2019).

After dynamic responses analysis, characteristic response values of the relevant limiting parameters could be estimated based on extreme value distributions for a target exceedance probability. According to the comparison between the characteristic value and the allowable limit of the limiting parameter, it is able to assess allowable sea states of the operation. Once allowable sea states are assessed, decisions on starting times of the operation could be made by comparing allowable sea states with weather forecasts in the execution phase. It is well known that the weather system is so complicated that it is difficult to be forecasted with high accuracy, and therefore uncertainty will be inherent in the weather forecasts. The accuracy of weather forecasts is normally assessed by comparing forecasted data with reference data from measurements or hindcasts. Then, the forecast error statistics can be calculated to quantify the forecast uncertainty at different forecast lead times. Typical error statistics include mean value and standard deviation, root mean square error (RMSE), scatter index (SI), correlation coefficient, etc. At present, a combination of multiple error statistics is mainly used to quantify the uncertainty in weather forecasts (Campos et al., 2021, 2022b). In order to reduce the uncertainty, the ensemble prediction systems have been produced in recent years. Compared with deterministic weather forecasts by a deterministic forecast model, the ensemble wave model performs probabilistic prediction by considering the possibilities for various initial conditions, wind forcing, boundary conditions and physical processes in physical wave models (Campos et al., 2020a; Molteni et al., 1996; Palmer, 2001) or machine learning (Campos et al., 2020b; O'Donncha et al., 2019). To measure the uncertainty in ensemble wave forecasts, in addition to typical error statistics, the ensemble mean and spread, brier score (BS) and reliability diagram are also applied as indicators (Harpham et al., 2016; Leutbecher and Palmer, 2008; Roh et al., 2021; Saetra and Bidlot, 2004). Different studies have proved that the ensemble forecasts performs better than the deterministic forecasts and are able to be regarded as a measure of the uncertainties in the deterministic forecasts (Campos et al., 2022a; Chen, 2006; Saetra and Bidlot, 2004).

Furthermore, how to reflect weather forecast uncertainty when performing marine operations is a key issue. This uncertainty will heavily affect the weather window predictions and further influence their decision-making. So far, only a few studies have been published on investigating the effect of weather forecast uncertainty on marine operations. At present, an alpha-factor α (a normalized factor less than 1) proposed by DNV (JIP, 2007) is normally used to downgrade the operational limit in terms of weather variables, in order to make the decision more conservative. In practice, this criterion is primarily expressed in terms of H_s and makes the operation's allowable sea state become $\alpha \bullet H_s$. However, in view of the current development of marine operations related to the OWTs installation, only accounting for H_s might not be sufficient since responses of the installation system also strongly depend on other weather variables such as the peak wave period T_p. In this case, Wu and Gao (2021) presented a similar indicator, called the response-based alpha-factor α_R, to reflect the effect of forecast uncertainties in both H_s and T_p on marine operations. This factor is generated from the perspective of dynamic response of the system and it is an operation-specific criterion. In that paper, a preliminary study on the response analysis of crane tip motions on a floating system was carried out by applying frequency-domain response analysis approach under different wave conditions, to illustrate the feasibility of the α_R. However, for the challenging blade installation, the nonlinear wind loads acting on the blade is also important and needs to be considered simultaneously. Hence, time-domain simulation is critical to numerically model the actual installation process and assess the dynamic responses of the blade during installation. The aim of the present study is to derive α_R for the offshore blade installation using a semi-submersible crane vessel on the basis of time-domain response analysis approach. Furthermore, allowable sea states of the corresponding mating operation are assessed with emphasis on taking into account the uncertainty of weather forecasts.

The paper is organized as follows. In Section 2, the procedure for derivation of α_R and assessment of allowable sea states for the offshore blade installation is presented. The forecast uncertainty quantification of H_s and T_p at the North Sea center are summarized in Section 3. Section 4 provides the details about the time-domain numerical modelling and dynamic response analysis of the blade installation using a semi-submersible vessel. According to the response time series, the extreme value distribution and characteristic value of two limiting response

parameters (i.e., blade root radial motion and velocity) are estimated by statistical analysis. Based on weather forecast analysis and dynamic response analysis, the α_R factors of each limiting response parameter are then generated and given in Section 5. The corresponding allowable sea states are assessed in Section 6. Finally, main conclusion and limitations are summarized in Section 7.

2. Assessment procedure

This section presents a procedure for assessing allowable sea states for offshore blade installation using time-domain numerical models and considering weather forecast uncertainty.

2.1. Planning phase

During the planning phase of the blade installation, numerical simulations of the operation should be conducted and dynamic responses of the structure should be assessed. These are necessary to evaluate the response-based alpha factor α_R (Wu and Gao, 2021), which is designed to account for the effect of forecast uncertainties in sea states (characterized by H_s and T_p) on dynamic responses of the coupled system for marine operations. The overall procedure to establish the α_R for offshore blade installation in time domain during the planning phase is briefly presented in Fig. 1 and the details are further discussed in the following. The blue parts in the figure are operation-specific conditions, which could be changed according to the properties of weather conditions and marine operations.

To establish the α_R for offshore blade installation, both weather forecast uncertainty analysis and dynamic response analysis are required.

2.1.1. Weather forecast uncertainty analysis

For weather forecast uncertainty analysis, the input parameters for weather forecasting and the forecasting method should be determined first, see steps 1-1 and 1–2 in Fig. 1. Sea state is normally characterized by H_s and T_p, which can be forecasted by means of various methods, such as the physics-based numerical method, the statistical method and the machine learning method. In this study, a machine learning-based method, called the physics-based machine learning (PBML) method (Wu et al., 2020), is utilized and the target forecast horizon is 24 h, referring to the typical execution duration of marine operations. Given that the sea state reference period T_S of the dataset used is 3 h, the forecast lead times T_L are 3 h, 6 h, etc., until 24 h. The adopted weather forecasting method (i.e., PBML) and dataset will be described in Section 3 in details. In addition, it should be noted that the weather forecast data from meteorological centers such as METOffice can also be utilized to perform weather forecast uncertainty analysis and establish the corresponding uncertainty model, in order to derive the response-based alpha-factor α_R. Such factor will depend on the accuracy of the forecasting method.

To quantify the forecast uncertainty, two forecast error factors ε_h and ε_t, defined as the ratio between the true and the forecasted values of H_s and T_p (as shown in step 1–3 and Eqs. (1) and (2)), will be used. They are assumed as random Gaussian variables that depend on the sea state ranges and the forecast lead time. By statistically analyzing forecast data, their distributions can be generated. Based on the expressions of ε_h and ε_t, actual H_s^t and T_p^t are also random Gaussian variables for a given forecasted h_s^f and t_p^f, and the forecast uncertainty distribution $f_{H_s^t T_p^t}(h_s^t, t_p^t)$ (step 1–4 in Fig. 1) will be established according to the generated error distributions. This distribution reflects the possibility of true sea states when a forecasted sea state is provided, and therefore reveals the weather forecast uncertainty. In addition, weather forecast analysis can also be carried out directly by applying commonly used error statistics (e.g., bias and correlation coefficient) of weather forecasts, which are normally provided by various forecasting institutions. This will be introduced in Section 3.

$$\varepsilon_h = \frac{H_s^t}{h_s^f} \tag{1}$$

$$\varepsilon_t = \frac{T_p^t}{t_p^f} \tag{2}$$

2.1.2. Dynamic response analysis

For dynamic response analysis, the critical events and corresponding limiting response parameters as well as the operation duration should be pre-identified for a specific operation, see step 2-1 in Fig. 1. Based on the analysis from Zhao (2019), the final mating process between the blade root and hub is critical for the blade installation, and the related critical

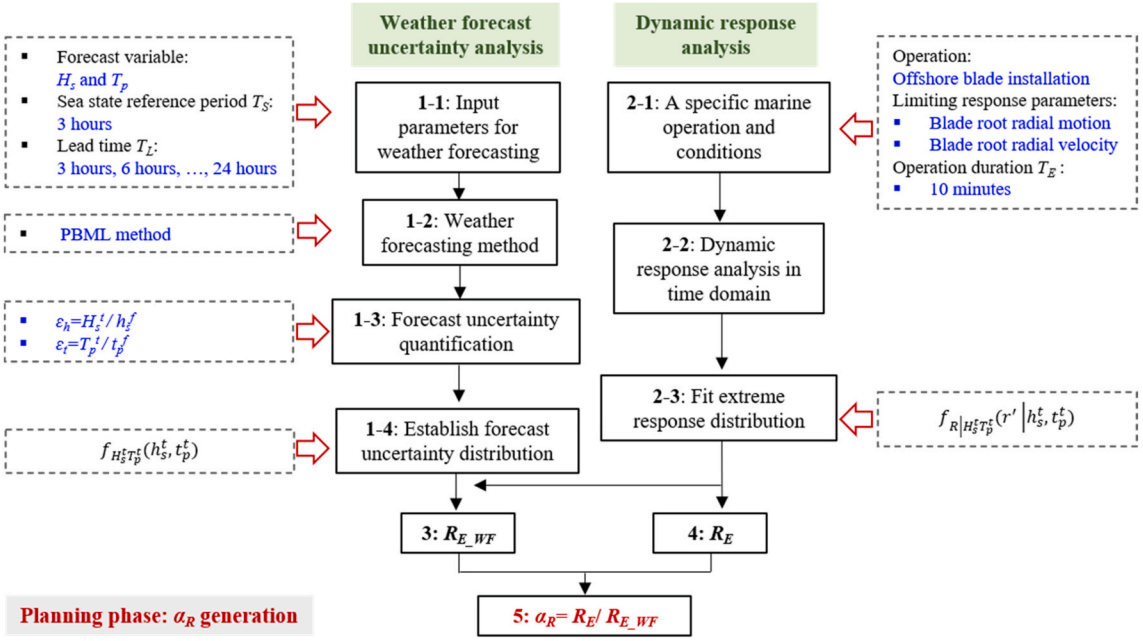

Fig. 1. Overview procedure for establishing α_R for offshore blade installation.

events are excessive radial motion of blade root and bent guide pins at blade root. Correspondingly, the limiting response parameters are the blade root radial motion and blade root radial velocity, respectively. For the identified limiting response parameters, dynamic responses can be obtained and analyzed by numerical modelling of the actual installation process in time domain (lasting about 10 min corresponding to the duration T_E of the mating process).

The dynamic response analysis in time domain shown in step 2-2 is more time-consuming than the analysis in frequency domain, since a large amount of time-domain simulations is required. In frequency domain, the response spectrum of a limiting response parameter for a given sea state can be estimated in terms of the transfer function and wave spectrum under a linear assumption. Accordingly, based on the statistical information derived from the response spectrum, the extreme value distribution can be established straightforwardly. By contrast, the extreme value distribution in time domain (step 2–3 in Fig. 1) should be fitted by means of a set of maximum response values. Specifically, for a given sea state, time-domain numerical simulations of blade installation should be conducted N times using different random wave seeds to obtain multiple response time series. By extracting the maximum value in each response time series, N independent response maxima can be obtained. They will be used to fit the extreme value distribution according to different methods, e.g., the maximum likelihood estimation method, the method of moments, etc. For different sea states, this procedure should be performed repeatedly to establish corresponding extreme value distributions. Although the use of time-domain response analysis approach requires high computational cost, it is necessary for the simulation of complex non-linear systems. These will be discussed in Section 4.2.

Based on the results of forecast uncertainty quantification and dynamic response analysis, the extreme value distributions of a limiting response parameter with and without weather forecast uncertainty for the given sea state can be obtained. Their cumulative density functions (CDFs) are given by Eqs. (3) and (4), denoted as $F_R(r)$ and $F_R^{WF}(r)$ respectively. From these two distributions, the characteristic responses corresponding to a target exceedance probability p can be calculated. R_E and R_{E_WF} (shown in steps 3 and 4 in Fig. 1) represent the characteristic values of the extreme responses with and without considering weather forecast uncertainty, that are calculated by Eqs. (5) and (6), respectively. Finally, the α_R for the given sea state can be calculated by Eq. (7) and shown in step 5. By following the procedure illustrated in Fig. 1, α_R corresponds to the blade root radial motion and velocity under different sea states can be obtained separately. In addition, it should be noted that in order to integrate Eq. (4), the conditional PDF of the extreme response $f_{R|H_s^t T_p^t}(r'|h_s^t, t_p^t)$ at different actual sea states (h_s^t, t_p^t) must be pre-identified. Since it is not realistic to cover all sea states, parameters in the extreme value distribution should be fitted in terms of H_s and T_p, which will be described in Section 4.3.

$$F_R(r) = \int_0^r f_{R|H_s^t T_p^t}\left(r' \middle| h_s^t, t_p^t\right) dr' \tag{3}$$

$$F_R^{WF}(r) = \int_0^r \int_0^{+\infty} \int_0^{+\infty} f_{R|H_s^t T_p^t}\left(r' \middle| h_s^t, t_p^t\right) \cdot f_{H_s^t T_p^t}\left(h_s^t, t_p^t\right) dh_s^t dt_p^t dr' \tag{4}$$

where $f_{R|H_s^t T_p^t}(r'|h_s^t, t_p^t)$ is the conditional probability density function (PDF) of the extreme response with a given actual sea state (h_s^t, t_p^t). $f_{H_s^t T_p^t}(h_s^t, t_p^t)$ reflects the uncertainty in actual sea state for a given forecasted sea state (h_s^f, t_p^f).

$$1 - F_R(R_E) = p \tag{5}$$

$$1 - F_R^{WF}(R_{E\_WF}) = p \tag{6}$$

where p is the exceedance probability, which depends on the type of operation, the consequences of failure, etc. 10^{-4} is normally considered for marine operations, which is recommended in the DNV standard (DNV, 2011).

$$\alpha_R = \frac{R_E}{R_{E\_WF}} \tag{7}$$

2.2. Execution phase

During the execution phase, decisions on whether or not to start the operation should be made. The basic criterion for decision-making is that the characteristic value of a limiting parameter should not exceed its allowable limit (Guachamin-Acero et al., 2016). In practice, for ease of use, the allowable limit is usually transformed into the limit in terms of sea state parameters, which is referred to the allowable sea states. A comparison of the weather forecast with the assessed allowable sea states can then support installation decision-making. To account for the weather forecast uncertainty, traditionally, the assessed allowable sea states in terms of H_s can be adjusted directly by the selected α when using the α-factor generated by DNV. That is, the new allowable sea states for an operation are considered to be $\alpha \bullet H_s$. In comparison, the α_R takes into account the forecast uncertainty in both H_s and T_p and is determined from the perspective of dynamic responses. Correspondingly, allowable sea states cannot be adjusted directly and have to be reassessed considering explicitly the forecast uncertainty. Fig. 2 shows two methods for dealing with the forecast uncertainty of H_s and T_p in decision-making during the execution phase.

The first method is to use the response-based alpha factor, which requires the direct response calculation in real time when the forecasted H_s and T_p were obtained and the forecasted responses are calculated. As shown in Fig. 2, the characteristic response R_E under a specific weather forecast (H_s, T_p) should be calculated. By using it with the α_R generated in the planning phase, the true responses R_{E_WF} considering the weather forecast uncertainty could be obtained in Eq. (7). Based on the comparison result between the R_{E_WF} and the allowable limit, decisions on whether to start the operation can be made. This is the similar method as the H_s-based alpha factor approach from DNV, but to correct responses.

The second method is to generate the contour plots. In this method, characteristic responses R_{E_WF} considering weather forecast uncertainty are calculated firstly under typical sea states using the method introduced in Section 2.1. Then based on the comparison between R_{E_WF} and the allowable limit, allowable sea states of an operation can be established. The allowable sea states are contour plots in terms of H_s and T_p, representing the maximum sea states that the operation can be safely executed. A simplified example is displayed in Fig. 2. The allowable sea states could be further used to make decisions on whether to start the installation. This is done by identifying workable weather windows based on the comparison between allowable sea states with weather forecasts. Obviously, once allowable sea states are generated in terms of H_s, T_p and lead times, it is quite convenience to use them. In this paper, allowable sea states of offshore wind turbine blade installation are assessed based on this method. In addition, it is important to emphasize that an operation may be governed by series of limiting response parameters. For example, in this paper, both blade root radial motion and blade root radial velocity govern the final mating phase simultaneously during the blade installation. In this case, weather windows corresponding to each limiting response parameter may affect the selection of execution time for the installation. Thus, weather windows for the two limiting response parameters should be identified individually, and the overall workable weather windows of the mating operation is the overlap part of them.

3. Weather forecasting and uncertainty quantification

The North Sea center, that is the central part of the North Sea, is

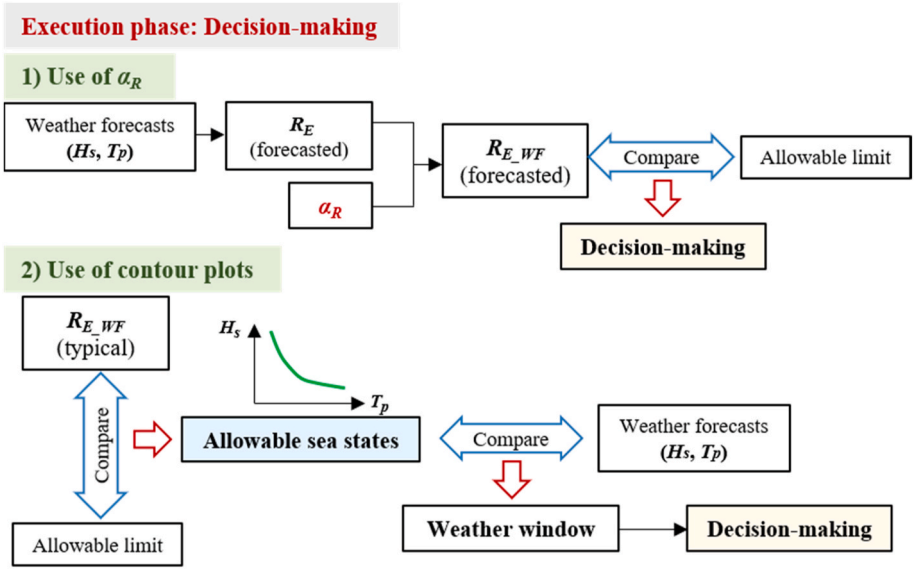

Fig. 2. Methods for decision-making considering weather forecast uncertainty in the execution phase.

selected as the target installation location. At this location, one-day-ahead H_s and T_p are forecasted respectively on the basis of the physics-based machine learning (PBML) method. The PBML method is a hybrid method, which designs the forecasting model with reference to the physical phenomena of wave evolutions embodied in physics-based wave models and employs machine learning technique to learn the model. The PBML models for H_s and T_p are trained separately, by nine years (2001–2009) three-hourly hindcast wave and wind data from the CERA-20C dataset (Laloyaux et al., 2018). After training successfully, H_s and T_p are forecasted by the trained models and their uncertainties are quantified based on the hindcast data in year 2010 from the same dataset. Since a sufficient number of the training and testing data is used, the effect of uncertainties from the ensembling could be reduced. For detailed description of the PBML method and the multi-step-ahead forecast results at the North Sea center, refer to Wu et al. (2020).

Fig. 3 shows the forecasted time series of H_s as well as the actual data (hindcast data used in the study). To illustrate the forecast performance, only the first 200 data during the testing period is plotted. Each one-day-ahead forecast case contains 8 forecasts, from one-step-ahead to eight-step-ahead. The green and blue points represent one- and eight-step-ahead forecast values respectively, representing the beginning and end of one forecast case. The next case starts when the previous one ends. Although good overall forecast performance can be seen, the forecast uncertainty is inevitable in the forecasting model. This phenomenon is more evident as the forecast step increases, presented by the deviation between the forecast data and the corresponding actual ones.

To quantify the weather forecast uncertainty, statistical analysis of the forecast results should be carried out. Since the offshore blade installation is often performed in relatively calm weather, the uncertainty of weather forecasts corresponding to low sea states is studied. Correspondingly, ε_h and ε_t are evaluated as functions of the range of h_s^f and t_p^f. As aforementioned, it is assumed that the forecast errors ε_h and ε_t follow Gaussian distributions. According to the definition of ε_h and ε_t, the PDFs of actual H_s^t and T_p^t, i.e., $f_{H_s^t}(h_s^t)$ and $f_{T_p^t}(t_p^t)$, also follow Gaussian distributions with adjusted mean values and standard deviations of the forecast errors, as shown in Eqs. (8) and (9) respectively. Given that H_s and T_p are forecasted separately, their uncertainties are assumed to be independent in the study, and the distribution of actual sea state can be expressed as Eq. (10). In addition, it should be noted that, if an ensemble forecast wave model is applied, statistics of the forecast errors (i.e., mean values and standard deviations) should be calculated based on the ensemble forecasts at a certain lead time.

$$f_{H_s^t}(h_s^t) = N\left(h_s^f \cdot \mu_{\varepsilon h},\ {h_s^f}^2 \cdot {\sigma_{\varepsilon h}}^2\right) \tag{8}$$

$$f_{T_p^t}\left(t_p^t\right) = N\left(t_p^f \cdot \mu_{\varepsilon t},\ {t_p^f}^2 \cdot {\sigma_{\varepsilon t}}^2\right) \tag{9}$$

$$f_{H_s^t T_p^t}\left(h_s^t, t_p^t\right) = f_{H_s^t}\left(h_s^t\right) \cdot f_{T_p^t}\left(t_p^t\right) \tag{10}$$

where $\mu_{\varepsilon h}$ and $\sigma_{\varepsilon h}$ are mean value and standard deviation of ε_h respectively. $\mu_{\varepsilon t}$ and $\sigma_{\varepsilon t}$ are mean value and standard deviation of ε_t respectively.

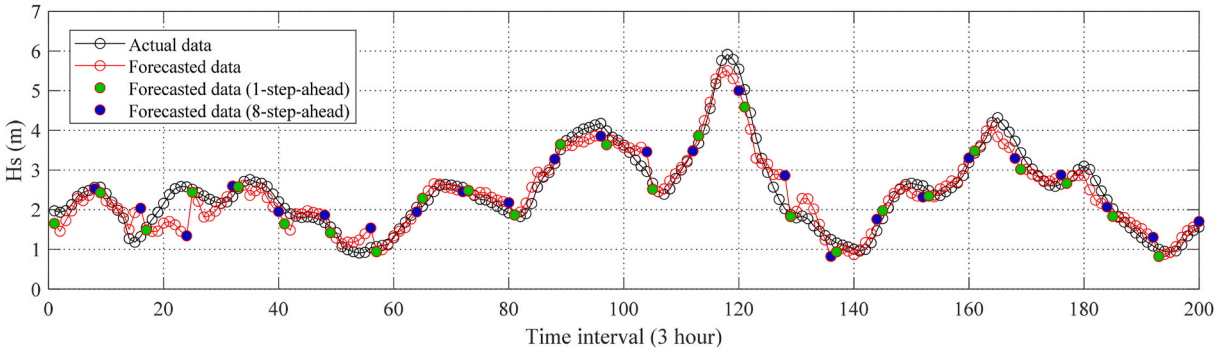

Fig. 3. Forecasted time series of H_s by means of the PBML method.

Forecast uncertainties of H_s and T_p using the PBML method have been quantified and discussed in Wu and Gao (2021). The results are summarized in Tables 1 and 2 respectively, which list the statistics of ε_h and ε_t in terms of the range of h_s^f and t_p^f as well as the forecast lead time T_L. These will be utilized to generate the α_R in the following part.

In addition to the PBML model employed in the study, physics-based wave models (such as WAM (Group, 1988), SWAN (Booij et al., 1999) and WATCH III (Tolman, 1991)) are another choice commonly used for the sea state forecasting. Various meteorological centers such as ECMWF (European Centre for Medium-Range Weather Forecasts) and MetOffice are able to provide sea state forecasts based on the physics-based wave models. Their forecast performance is generally evaluated in terms of error statistics like RMSE, bias, SI, etc. In order to deal with the corresponding forecast uncertainty and apply the results in the development of α_R, a slightly different uncertainty model should be developed. The aim of the model is to directly use error statistics for the uncertainty quantification analysis.

In this uncertainty model, the forecast error Δ_h and Δ_t for H_s and T_p are used in the forecast uncertainty analysis, which are shown in Eqs. (11) and (12) respectively. Likewise, they are also modelled as random Gaussian variables but considering all possible forecasted sea states. As a consequence, Δ_h and Δ_t are not functions of the sea state ranges, but only functions of the forecast lead time. This is the different as compared to the error factors defined in Eqs. (1) and (2). To establish their distributions, the corresponding Gaussian parameters (i.e., the mean value μ_Δ and standard deviation σ_Δ) can be derived directly by means of RMSE and bias instead of statistical analysis of forecasted data. Their expressions can be seen in Eqs. (13) and (14), respectively.

$$\Delta_h = h_s^f - H_s^t \tag{11}$$

$$\Delta_t = t_p^f - T_p^t \tag{12}$$

$$\mu_\Delta = bias \tag{13}$$

$$\sigma_\Delta = \sqrt{RMSE^2 - bias^2} \tag{14}$$

A detailed example will show the work of it in the following part. Table 3 summarizes the forecast performance of one-day-ahead H_s and T_p in terms of RMSE and bias. In the table, physics-based numerical methods from six forecast modelling institutions are considered, namely ECM (ECMWF), MOF (MetOffice), MTF (MeteoFrance), SHM (SHOM - Service hydrographique et océanographique de la Marine, Naval Hydrographic and Oceanographic Service), DMI (Danish Meteorological Institute) and MTN (METNO). The results are extracted from a report (JR, 2017), which evaluated the forecast accuracy of H_s and T_p by comparing the forecasts against measurements at different North Sea buoys.

Following the above procedure, the calculated statistics of Δ_h and Δ_t are listed in Table 4. According to the expressions of Δ_h and Δ_t, the conditional PDFs of actual H_s and T_p can be expressed as Eqs. (15) and (16), respectively. Then the distribution of actual sea state is estimated by Eq. (10). By doing this, the evaluation information of weather forecasts issued by different forecast modelling institutions can be used, and the forecast uncertainty quantification can therefore be carried out. The quantification results will be further used in the following allowable sea state assessment. However, this is a relatively simple method since the error keeps constant within all ranges of the weather variables, and the error distributions are not expressed as a function in terms of h_s^f and t_p^f. Then the distribution of actual sea state can be estimated by Eq. (10). By doing this, the evaluation information of weather forecasts issued by different forecast modelling institutions can be used, and the forecast uncertainty quantification can be carried out. The quantification results can be further used in the following allowable sea state assessment.

However, this is a relatively simple method since the error keeps constant within all ranges of the weather variables, and the error distributions are not expressed as a function in terms of H_s^f and T_p^f.

4. Dynamic response analysis of the single blade installation

4.1. Numerical model and simulation method

This study focuses on the final mating phase of single blade installation. In this phase, the blade is close to the nacelle and the dynamic properties of the system do not vary with time significantly. Therefore, the steady-state analysis of blade installation is performed. The configuration of a semi-submersible crane vessel used to simulate the single blade installation is shown in Fig. 4. As displayed, the numerical model consists of three main parts, i.e., a semi-submersible vessel, a crane and a blade. The semi-submersible vessel is assumed to be equipped with dynamic positioning (DP) systems to mitigate its slowly varying motions in surge, sway and yaw. The crane is modelled as the typical pedestal crane and the DTU 10 MW wind turbine blade (Bak et al., 2013) is used. Detailed description of dimensions and dynamic properties of the system can be found in Zhao et al. (2019) and Wu and Gao (2021). Three right-handed coordinate systems, i.e., a global coordinate system O-XYZ, a vessel-related coordinate system O_v-$X_vY_vZ_v$ and a blade-related coordinate system O_b-$X_bY_bZ_b$, are applied in the study, whose origins are located at the mean sea surface, the center of the waterplane of the semi-submersible at rest and the center of gravity (COG) of the blade, respectively. X_v and X_b are in the longitudinal direction of the vessel and blade, respectively. In the initial stage, the latter two local coordinate

Table 1
Statistics of ε_h in terms of different H_s groups and forecast lead times.

Statistical parameter	h_s^f group (m)	Forecast lead time (hour)							
		3	6	9	12	15	18	21	24
$\mu_{\varepsilon h}$	0.5	0.97	0.94	0.98	0.98	0.98	0.98	0.99	0.99
	1.0	1.02	1.02	1.01	1.01	1.01	1.00	1.00	1.00
	1.5	1.02	1.01	1.01	1.01	1.00	1.00	0.99	0.99
	2.0	1.03	1.02	1.01	1.01	1.00	1.00	0.99	0.98
	2.5	1.00	1.01	1.00	1.00	0.99	0.99	0.99	0.98
	3.0	0.99	0.99	0.99	0.99	0.99	0.99	0.99	0.99
	3.5	0.98	0.99	0.99	0.99	1.00	1.00	1.01	1.02
	4.0	0.95	0.96	0.96	0.97	0.98	0.99	1.00	1.00
$\sigma_{\varepsilon h}$	0.5	0.12	0.13	0.15	0.16	0.17	0.19	0.20	0.22
	1.0	0.11	0.13	0.15	0.17	0.20	0.22	0.24	0.26
	1.5	0.10	0.12	0.14	0.16	0.18	0.20	0.22	0.24
	2.0	0.09	0.11	0.12	0.14	0.14	0.17	0.19	0.20
	2.5	0.08	0.09	0.10	0.11	0.13	0.14	0.15	0.17
	3.0	0.09	0.09	0.10	0.11	0.12	0.13	0.13	0.14
	3.5	0.07	0.08	0.09	0.10	0.11	0.12	0.14	0.15
	4.0	0.09	0.09	0.10	0.10	0.11	0.14	0.12	0.12

Table 2
Statistics of ε_t in terms of different T_p groups and forecast lead times.

Statistical parameter	t_p^f group (s)	Forecast lead time (hour)							
		3	6	9	12	15	18	21	24
$\mu_{\varepsilon t}$	5	1.02	1.03	1.05	1.06	1.08	1.09	1.11	1.12
	6	0.98	0.99	0.99	1.00	1.00	1.01	1.00	1.02
	7	1.01	1.01	1.00	1.00	1.00	1.00	1.00	0.99
	8	1.00	1.00	1.00	1.00	1.00	1.00	0.99	0.99
	9	1.00	1.00	0.99	0.98	0.98	0.97	0.97	0.96
	10	1.00	1.00	0.99	0.99	0.98	0.98	0.97	0.97
$\sigma_{\varepsilon t}$	5	0.24	0.25	0.26	0.27	0.28	0.29	0.29	0.30
	6	0.15	0.16	0.17	0.18	0.19	0.19	0.20	0.21
	7	0.11	0.13	0.14	0.15	0.16	0.17	0.18	0.19
	8	0.12	0.13	0.13	0.14	0.15	0.16	0.17	0.17
	9	0.13	0.13	0.14	0.14	0.14	0.15	0.15	0.16
	10	0.11	0.11	0.12	0.12	0.13	0.13	0.14	0.14

Table 3
Error measures of one-day-ahead H_s and T_p forecasts.

Forecast modelling institutions	Forecast variable			
	H_s		T_p	
	bias	RMSE	bias	RMSE
ECMWF	−0.15	0.32	−0.35	0.84
MOF	−0.08	0.25	−0.08	0.84
MTF	−0.22	0.42	−0.22	1.02
SHM	−0.27	0.44	−0.44	0.84
DMI	−0.11	0.27	−0.28	1.26
MTN	−0.17	0.29	−0.26	0.84

systems are parallel to the global one.

The offshore blade installation is simulated by a fully coupled simulation method SIMO-RIFLEX-Aero (Zhao et al., 2018b) in time-domain, which integrates three programs, i.e., SIMO (SINTEF Ocean (2017)), RIFLEX (SINTEF Ocean (SINTEF, 2017)) and Aero code (Zhao et al., 2018a). Among them, the hydrodynamic loads on the semi-submersible and structural dynamics (e.g., crane flexibility) are analyzed by SIMO and RIFLEX respectively, and they are integrated in the SIMA workbench (SINTEF, 2015). The aerodynamic loads acting on the blade are calculated by the Aero code based on the cross-flow principle (Hoerner and Borst, 1975; Horner, 1965), in terms of the instantaneous blade displacement and velocity at each time step. It is coupled with SIMO and RIFLEX using the external dynamic link library (DLL) in SIMA.

During the mating phase of the blade onto hub, the blade root radial

Table 4
Error mean and standard deviation of forecasts from six institutions ($T_L = 24$ h).

$$f_{H_s^t|H_s^f}\left(h_s^t|h_s^f\right) = N\left(h_s^f - \mu_{\Delta h},\ {\sigma_{\Delta h}}^2\right) \tag{15}$$

$$f_{T_p^t|T_p^f}\left(t_p^t|t_p^f\right) = N\left(t_p^f - \mu_{\Delta t},\ {\sigma_{\Delta t}}^2\right) \tag{16}$$

Forecast variable	Gaussian parameter	Forecast modelling institutions					
		ECM	MOF	MTF	SHM	DMI	MTN
H_s	$\mu_{\Delta h}$	−0.15	−0.08	−0.22	−0.27	−0.11	−0.17
	$\sigma_{\Delta h}$	0.28	0.24	0.36	0.35	0.25	0.24
T_p	$\mu_{\Delta t}$	−0.34	−0.08	−0.22	−0.44	−0.28	−0.26
	$\sigma_{\Delta t}$	0.77	0.84	1.00	0.72	1.23	0.80

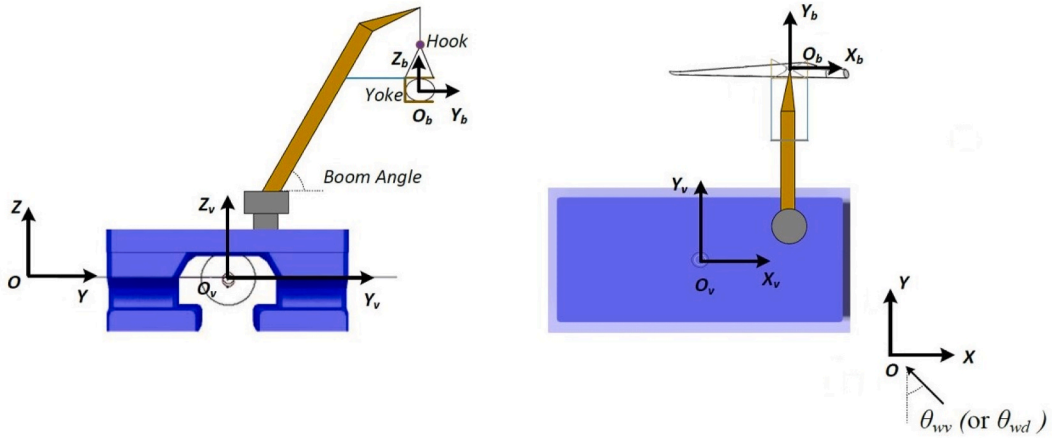

Fig. 4. Schematic view of the offshore blade installation system (θ_{wv} is the incident wave angle and θ_{wd} is the wind inflow angle).

motion and velocity (i.e., motion and velocity in the $Y_bO_bZ_b$ plane in Fig. 4) are very critical. To assess their dynamic responses, steady-state time-domain simulations are carried out under different wave and wind conditions. In this study, only irregular beam wind and wave conditions are considered (i.e., θ_{wv} and θ_{wd} are zero) because they could induce relatively higher response of the system. In addition, the JONSWAP spectrum with a peakness factor γ of 3.3 (Veritas, 2010) is used to describe sea states at the North Sea center.

4.2. Comparison between frequency and time domain analysis

The necessity of numerical simulation in time domain (TD) is discussed and illustrated in this section through a comparison with the results in frequency domain (FD). Fig. 5 shows the motion spectra of the semi-submersible in 6°-of-freedoms (DOFs) under a typical beam sea (H_s = 1 m and T_p = 7 s).

As illustrated in Fig. 5, in the beam sea condition, the sway and roll motions of the semi-submersible are relatively larger. The 1st order wave force dominant the motions, since the peak frequency in the motion spectrum is similar to the one of the wave spectrum. From a comparison with the results in FD and TD, a good agreement can be observed in the wave-frequency part. Nevertheless, in this study, the method in FD do not capture the slow varying motions (dominated by the difference frequency wave forces), which makes its power spectral density different from that of the motions obtained by the method in TD. This difference will further affect motions of crane tip and blade. The difference between power spectra of the crane tip motions is shown in Fig. 6. By comparison, the difference between the slow varying motions of the crane tip can also be observed in FD and TD.

The advantages and disadvantages of the method in TD and FD are briefly listed in Table 5. As shown above, the time domain modelling can capture the crane vessel motion which is subjected to wave loads more accurately by including nonlinear effects such as 2nd order wave forces, lift wire tension formulation and geometrical nonlinearities for motion analysis. Furthermore, the nonlinear aerodynamic loads on the blade and the strong coupling between waves and wind are also important for the response of the installation system. However, these cannot be directly included by the method in FD. Therefore, although its computational efficiency is relatively low, the time-domain modelling is necessary to simulate the whole blade installation process and perform dynamic response analysis.

4.3. Sensitivity analysis of wind loads

To establish the conditional distribution of the extreme response with a given sea state (i.e., $f_{R|H_s^t,T_p^t}(r|h_s^t,t_p^t)$), the time domain simulation has to be repeated many times with different wave seeds. As a consequence, it is time-consuming compared with the simulation in frequency domain. Moreover, different combinations of wind and wave conditions should be considered. Given that under each combination multiple simulations are required, the computational cost of extreme response analysis will be heavily increased. To decrease the cost in TD, a sensitivity study on wind loads will be carried out.

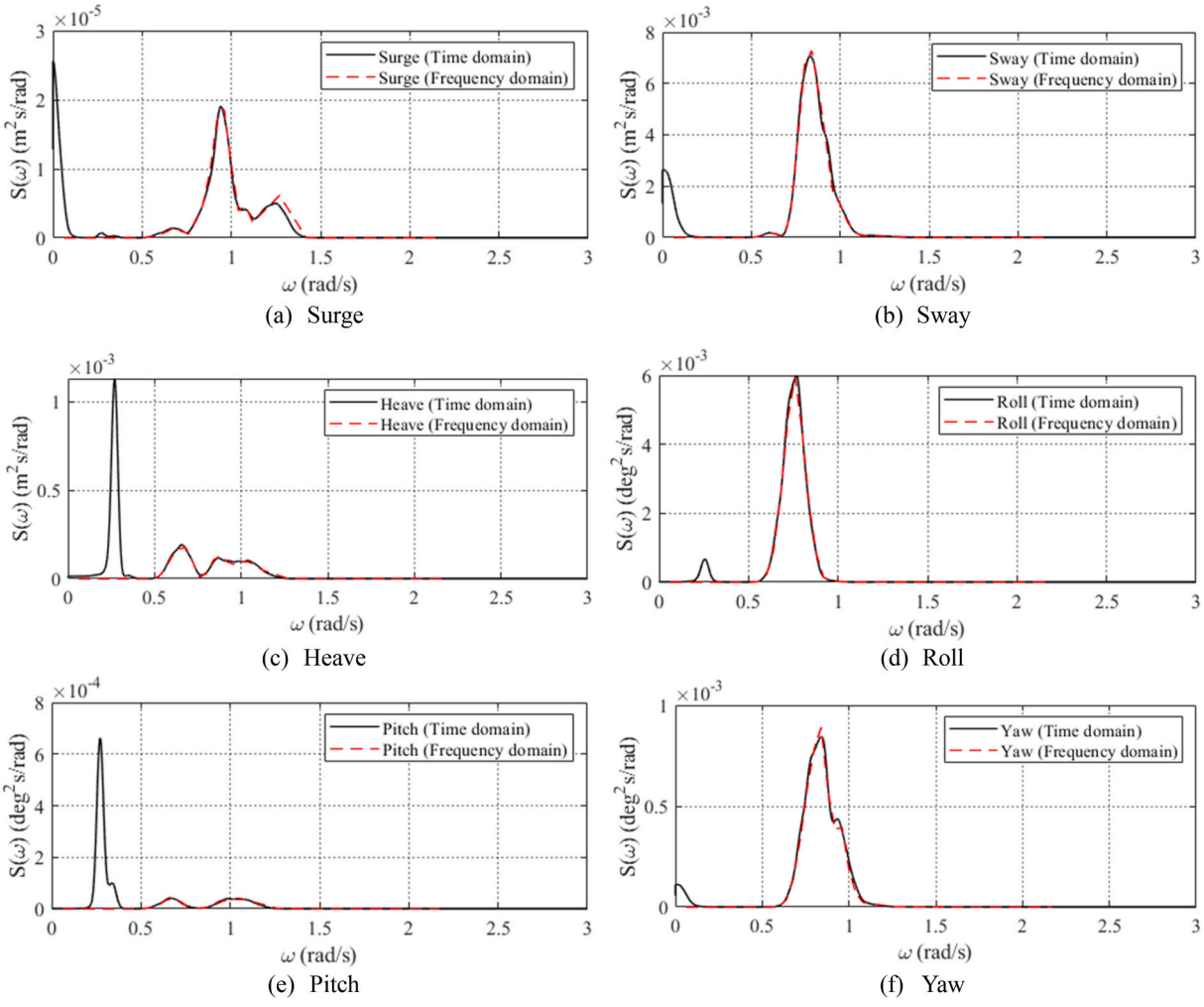

Fig. 5. Comparison of power spectra of semi-submersible motion using FD and TD methods (H_s = 1 m, T_p = 7 s).

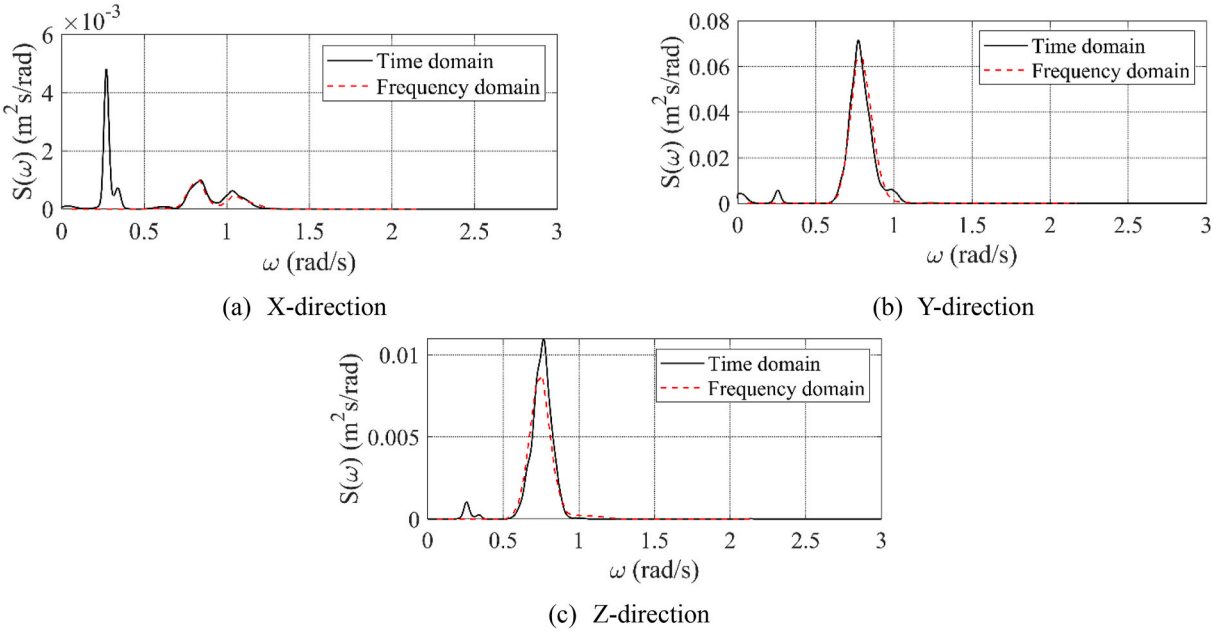

Fig. 6. Comparison of power spectra of crane tip motion using FD and TD methods (H_s = 1 m, T_p = 7 s).

Table 5
Properties of TD and FD response analysis methods for blade installation.

Response analysis methods	Advantage	Disadvantage	Properties of the modelling of blade
Time domain	Can simulate the whole blade installation process Various terms can be included: • 2nd order wave forces (mean drift and difference frequency wave forces) • Wind loads • Viscous loads • Nonlinear structural responses	Low computational efficiency	The actual blade root motion and velocity can be simulated, which are directly related to the operational criteria for installing blade
Frequency domain	High computational efficiency	Only includes 1st order wave loads and the linear motion response	The crane tip motion is referred to, not the blade motion

In the sensitivity study, a constant H_s value of 2 m is applied, and T_p is selected as the mean value of the conditional distribution of T_p with the given H_s value, which is 7.5 s. The conditional distribution of T_p with given H_s is modelled as a Lognormal distribution, in which the Lognormal parameters are fitted using ten-year hindcast data from the CERA-20C dataset at the target location. Likewise, the joint distribution of U_w, H_s and T_p is fitted by data based on a simplified method proposed by Li et al. (2015). The joint distribution is used to determine the mean wind speed distribution with the given sea state. From the mean wind speed distribution, five typical U_w values (i.e., 1.9 m/s, 3.6 m/s, 5.3 m/s, 7 m/s, 8.7 m/s) are selected to conduct the sensitivity study. It should be noted that the mean wind speed in the joint distribution is at the height of 10 m above the mean sea level. For offshore wind turbine installation, the mean wind speed at the hub height is required and it can be calculated using a power law profile shown in Eq. (17).

$$U(z) = U_{10} \cdot \left(\frac{z}{10}\right)^{\alpha_U} \tag{17}$$

where z represents the hub height, that is 119 m for the DTU 10 MW wind turbine. U_{10} is the mean wind speed at the reference height of 10 m α_U is the power law exponent which is set to 0.14 in this study, based on IEC 61400-3 (IEC, I., 2009) for an offshore wind field.

Substituting the parameters into Eq. (17), U_w values at the hub height are 2.7 m/s, 5.1 m/s, 7.5 m/s, 9.9 m/s and 12.3 m/s. For each U_w, the 3D turbulent wind field is generated by TurbSim (Jonkman and Buhl Jr, 2007) using the IEC Kaimal model (TC88-MT, 2005), and the turbulence intensity is defined as class C according to the standard IEC categories. The wind field is incorporated into SIMA using DLL to simulate the blade installation in time domain. After simulations, the power spectra and standard deviation of the blade COG motion in 6 DOFs with different wind fields are shown in Figs. 7 and 8 respectively. According to the blade COG motion, the radial motion of the blade root can be obtained. The power spectra and standard deviations of the blade root radial motion are shown in Fig. 9.

From Figs. 7 and 8, it is visible that the surge, heave and pitch motions of the blade COG are almost irrelevant to the wind in the beam wind and wave conditions, and the wave-induced motion is the main source of the blade motion in these 3 DOFs. By comparison, both aerodynamic loads and wave-induced motions contribute to the blade motion in sway, roll and yaw. Among them, the aerodynamic loads have significant effects on the blade roll motion and an obvious increase of the peak roll motion can be observed as the mean wind speed increases. Nevertheless, regarding radial motion of the blade root, it does not vary greatly under different wind conditions. Fig. 9 indicates that the wave loads have a major contribution on the blade root radial motion, while the aerodynamic loads have relatively less contribution.

Overall, the sensitivity study demonstrates that the wave load dominates over the wind load. From the perspective of computational efficiency, the mean wind speed is simply selected as a constant value (8 m/s at 10 m height) and the effect of different wind conditions on the blade installation is not considered in this paper.

4.4. Extreme response analysis

As aforementioned, unlike the extreme response analysis based on response spectra in frequency domain, the extreme value distribution in time domain needs to be fitted using maxima values extracted from the response time series. Fig. 10 shows a typical example of the extreme

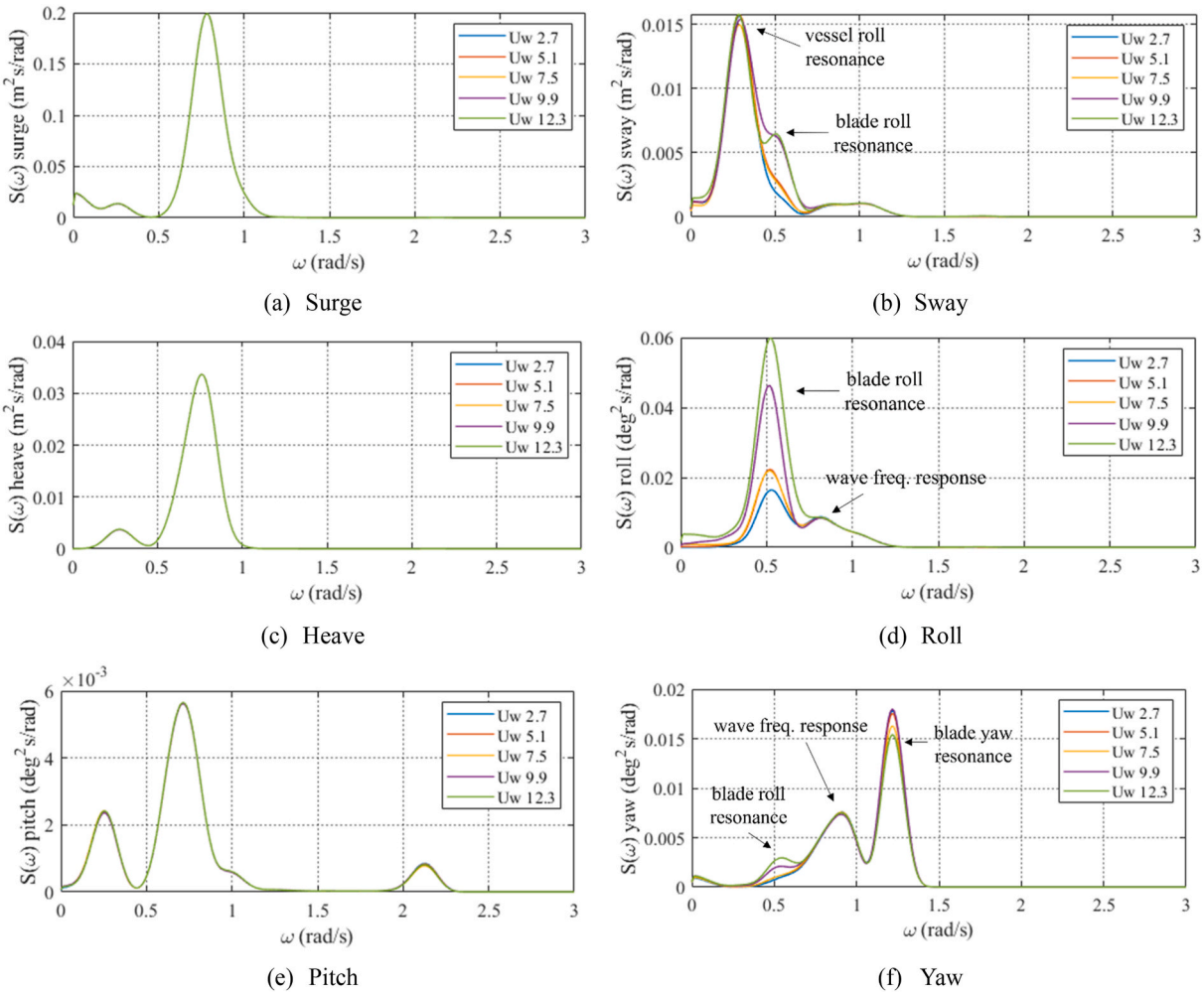

Fig. 7. Power spectra of blade COG motion with different wind fields ($H_s = 2$ m, $T_p = 7.5$ s).

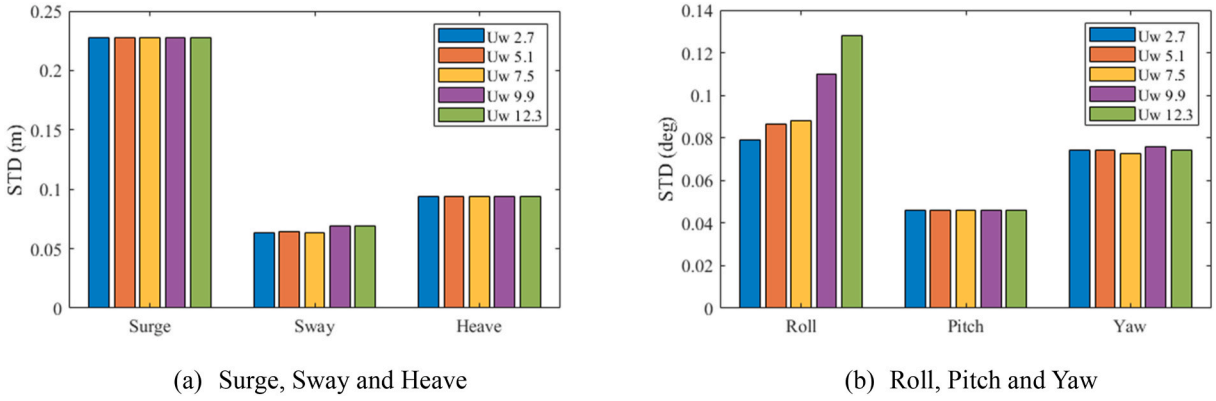

Fig. 8. Standard deviations of blade COG motion with different wind fields ($H_s = 2$ m, $T_p = 7.5$ s).

distribution of the blade root radial motion under a given sea state ($H_s =$ 2 m and $T_p = 5$ s). To reduce statistical uncertainty in the tail of the fitted distribution, 50 10-min time-domain simulations are carried out with random wave seeds. The Gumbel distribution is utilized to fit the extracted 10-min extreme responses.

Under this sea state, parameters (i.e., the location parameter γ and scale parameter β) of the Gumbel distribution are estimated by the maximum likelihood estimations (MLEs) method. Results shown in Fig. 10 (a) indicate that the Gumbel distribution has a good performance to capture the extreme radial motion of the blade root. The characteristic value can therefore be obtained based on the distribution with a certain exceedance probability, as shown in Fig. 10 (b). The exceedance probability refers to the failure probability per marine operations. In the mating phase of the blade installation, a small exceedance probability (i.e., 10^{-4}) is considered since larger radial motion and velocity of the blade root may lead to the failure of installation. In addition to 10^{-4}, other exceedance probability levels such as 10^{-2}, can also be used by taking the consequences of operation failure into account.

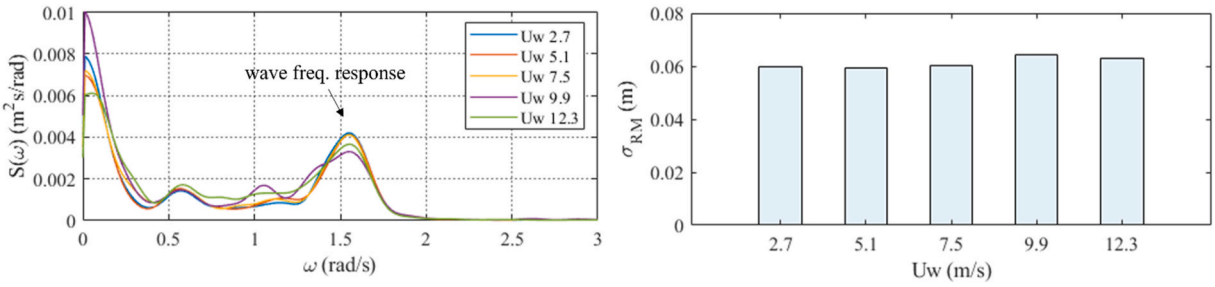

(a) Power spectra (b) Standard deviations

Fig. 9. Comparison of blade root radial motion with different wind fields ($H_s = 2$ m, $T_p = 7.5$ s).

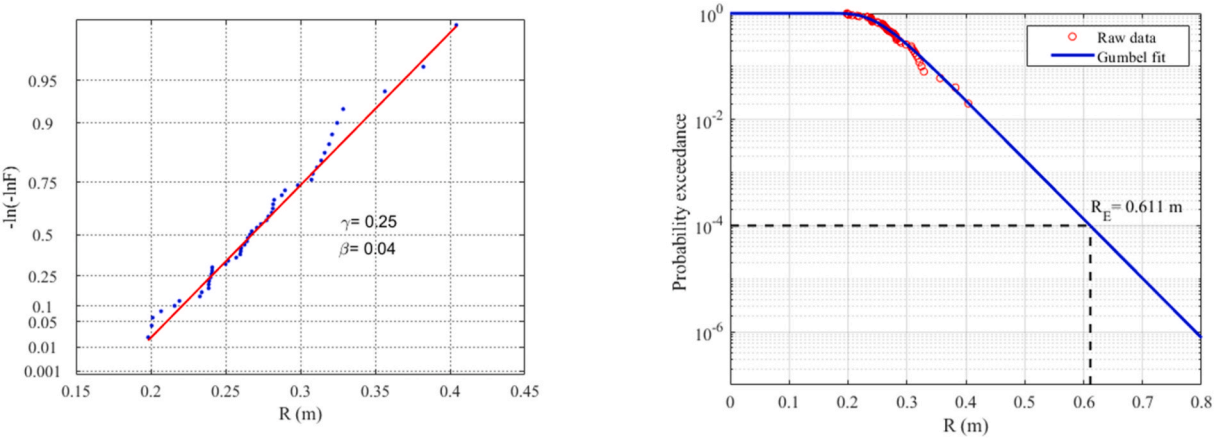

(a) Gumbel fitting (b) Exceedance probability

Fig. 10. Extreme value distribution estimation of the blade root radial motion (50 simulations, $H_s = 2$ m, $T_p = 5$ s).

4.4.1. Statistical uncertainty

In the above extreme response analysis, only a limited number of simulations (i.e., 50 10-min) are conducted to estimate the characteristic values with a quite small exceedance probability level. The statistical uncertainty may exist when fitting the extreme response distribution. In this subsection, the accuracy of the estimated extreme values due to a limited number of simulations is addressed.

In Fig. 11, the extreme distribution of the blade root radial motion under the given sea state ($H_s = 2$ m and $T_p = 5$ s) is further fitted, using 1000 simulations with different wave seeds. Based on the distribution, characteristic values with two exceedance probability levels, namely 10^{-2} and 10^{-4}, are estimated and displayed. For the 10^{-2} level, 1000 simulations can be considered as a reasonable choice, and the corresponding characteristic value is regarded as an accurate estimation for extreme responses. In this sensitivity study, the characteristic value with 10^{-4} level shown in Fig. 11 is also taken as the reference value for the extreme response. Comparison between Figs. 10 and 11 shows that there is a slight difference in the characteristic value estimated by different numbers of simulations.

To investigate the effect of simulation numbers in the extreme response analysis, Fig. 12 shows variation of the characteristic values of the blade root radial motion with the number of time-domain simulations. Results for the exceedance probability of 10^{-2} and 10^{-4} are displayed in subfigure (a) and (b) separately.

It is visible that the number of simulations affects the determination of fitting parameters for the Gumbel distribution, and thereby affect the estimation of the characteristic values. This phenomenon is especially obvious when the simulation number is less than 40. Compared with the case based on 1000 simulations, large uncertainty exists when only 5 simulations are used to estimate the extreme response. As expected, the

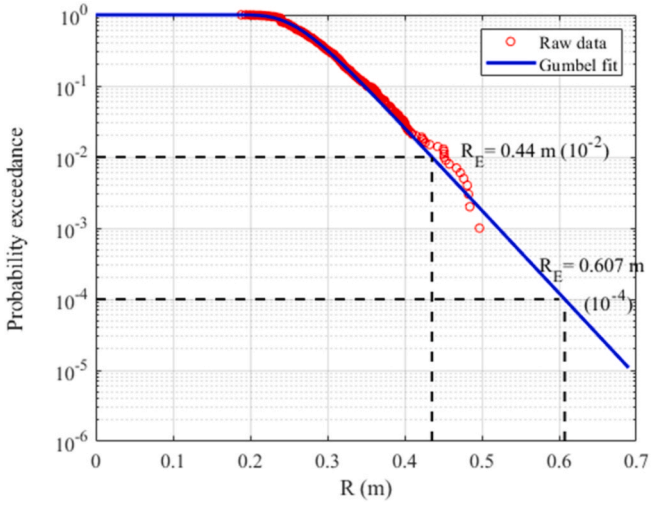

Fig. 11. Fitted extreme distribution of the blade root radial motion (1000 simulations, $H_s = 2$ m, $T_p = 5$ s).

statistical uncertainty decreases as the number of simulations increases. When the number of simulations is greater than 40, there is no significant difference in the results among different cases. Therefore, taking into account the computational efficiency, the number of simulations is selected as 50, which can give a reasonably good estimation of the characteristic response value.

Moreover, the statistical uncertainty of the extreme response

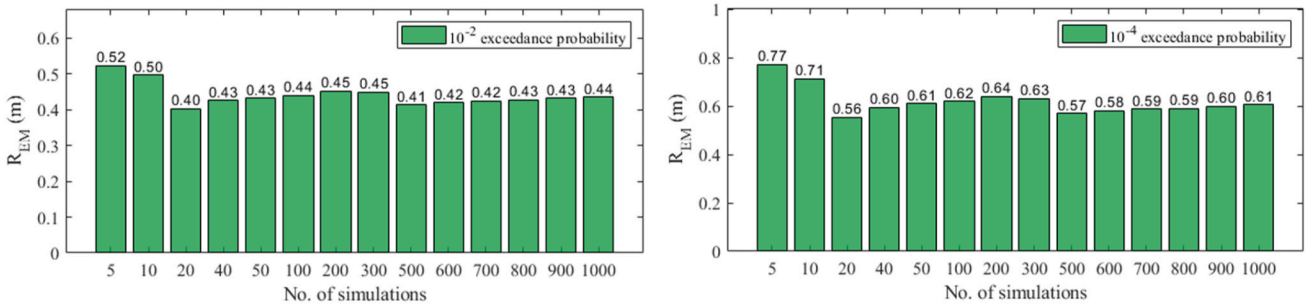

(a) Ten-min extreme response with a 10^{-2} exceedance probability

(b) Ten-min extreme response with a 10^{-4} exceedance probability

Fig. 12. Variation of the characteristic with the number of simulations (H_s = 2 m, T_p = 5 s).

assessed by a fixed number of simulations (i.e., 50) is illustrated in Fig. 13. In the figure, 10 sets of 50 time-domain simulations are selected randomly from 1000 simulations, and the extreme value in each set is estimated individually.

As illustrated, the variation in characteristic values between different sets is small. The coefficient of variation (*CoV*), that is defined as Eq. (18) in terms of the mean value (μ_{R_E}) and standard deviation (σ_{R_E}) of characteristic values, is applied to measure the related statistical uncertainty. It is calculated based on 20 sets of 50 time-domain simulations and the relevant results are summarized in Table 6. The results show low statistical uncertainty, since small *CoV* values corresponding to 10^{-2} and 10^{-4} exceedance probability levels (i.e., 4% and 6%) are observed.

$$CoV = \frac{\sigma_{R_E}}{\mu_{R_E}} \tag{18}$$

Overall, the fitted distribution with 50 simulations for a sea state can give an overall good estimation of the extreme value and the statistical uncertainty is low. Therefore, the extreme responses of both the blade root radial motion and velocity in this paper are assessed based on 50 time-domain simulations for each sea state.

Table 6
Statistical uncertainty in extreme response estimation (H_s = 2 m, T_p = 5 s).

Exceedance probability	μ_{R_E}	σ_{R_E}	*CoV*
10^{-2}	0.43	0.02	0.04
10^{-4}	0.59	0.03	0.06

Table 7
R_E values (in m) of the blade root radial motion (R_{EM}).

H_s (m)	T_p (s)					
	5	6	7	8	9	10
0.5	0.20	0.27	0.37	0.42	0.47	0.54
1.0	0.23	0.46	0.60	0.81	0.88	1.03
1.5	0.36	0.71	0.96	1.26	1.42	1.55
2.0	0.61	1.03	1.41	1.76	2.02	2.16
2.5	0.93	1.44	1.95	2.35	2.74	2.86
3.0	1.30	1.93	2.62	3.06	3.64	3.68
3.5	1.72	2.53	3.37	3.90	4.62	4.56
4.0	2.20	3.18	4.21	4.87	5.68	5.46

4.4.2. Characteristic response values

By carrying out the extreme response analysis in TD, the R_E values of the blade root radial motion and velocity under different typical sea states are calculated and summarized in Tables 7 and 8, respectively.

As displayed in Tables 7 and 8, R_{EM} and R_{EV} increase significantly with H_s and T_p. This indicates that both H_s and T_p are important for assessing the dynamic responses of the blade and need to be considered before executing the offshore blade installation. As aforementioned, the Gumbel parameters are functions of H_s and T_p. Figs. 14 and 15 present the fitting surfaces of Gumbel parameters for extreme radial motion and velocity of the blade root, respectively.

In Figs. 14 and 15, the blue points are Gumbel parameters estimated by the simulated response time series under typical sea states. They are utilized to evaluate the characteristic values without weather forecast uncertainty, i.e., R_E in Eq. (5). Based on these blue points, the surfaces of γ and β for different sea states are fitted by the piecewise cubic interpolation method (Fritsch and Carlson, 1980) in Matlab. These surfaces are necessary to integrate the marginal distribution of the extreme response expressed in Eq. (4). Accordingly, the characteristic values R_{E_WF} of the extreme radial motion and velocity can be calculated,

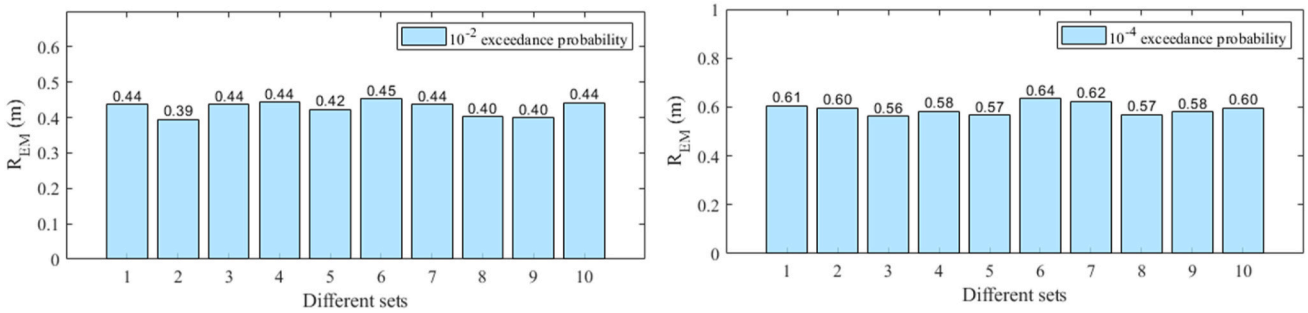

(a) Ten-min extreme response with a 10^{-2} exceedance probability

(b) Ten-min extreme response with a 10^{-4} exceedance probability

Fig. 13. Variation of the characteristic values in different sets (H_s = 2 m, T_p = 5 s).

Table 8
R_E values (in m) of the blade root radial velocity (R_{EV}).

H_s (m)	T_p (s)					
	5	6	7	8	9	10
0.5	0.13	0.18	0.25	0.27	0.31	0.33
1.0	0.22	0.36	0.47	0.58	0.61	0.64
1.5	0.32	0.53	0.70	0.88	0.98	0.96
2.0	0.43	0.70	0.92	1.19	1.22	1.29
2.5	0.54	0.88	1.16	1.50	1.53	1.62
3.0	0.66	1.06	1.40	1.82	1.84	1.94
3.5	0.78	1.24	1.66	2.15	2.17	2.28
4.0	0.90	1.43	1.92	2.48	2.49	2.63

accounting for weather forecast uncertainty by Eq. (6).

5. Response-based alpha-factor

Based on characteristic values of each limiting response parameter with and without weather forecast uncertainty, the response-based alpha-factors of the blade root radial motion (α_{RM}) and velocity (α_{RV}) can be estimated. Relevant results will be presented and discussed in this section.

5.1. Blade root radial motion

Fig. 16 shows an example of the α_{RM}, considering weather forecast uncertainty of the PBML method with a lead time of 3 h. It is clearly that the α_{RM} varies with sea states. Since the blade installation normally requires low sea states, Fig. 17 further presents the variation of α_{RM} for different T_p and T_L, focusing on the results in H_s ranging from 0.5 m to 2.0 m.

It is seen from Fig. 17 that the α_{RM} does not change significantly with the lead time, due to the good forecast performance of the PBML method on sea state forecasting. By comparing α_{RM} in different subfigures, a significant effect of forecast uncertainty in T_p is observed. Moreover, the effect of H_s can be found by comparing α_{RM} factors at each lead time for each subfigure. As shown, the α_{RM} varies with H_s, but the variation also depends on conditions of T_p and T_L.

5.2. Blade root radial velocity

A similar analysis is conducted on the blade root radial velocity. α_{RV} with different H_s, T_p and T_L are presented in Fig. 18. Likewise, only results in H_s groups between 0.5 m and 2.0 m are displayed.

From Fig. 18, the influence of T_p on the α_{RV} can be clearly found. For all lead times and H_s groups, α_{RV} are in the range of 0.16–0.52 for the T_p group of 5 s, and 0.52 to 0.99 for other T_p groups. By comparing Figs. 17 and 18, it is noted that the variation observed in α_{RV} is different from that observed in α_{RM}. This reflects the characteristics of α_R, that is, it is specific to the operations and associated limiting response parameters.

Overall, results demonstrate that for the blade installation using a floating crane vessel, uncertainty in T_p forecasts is important and should not be neglected. Therefore, it is meaningful to propose a correction factor α_R. Unlike the conventional alpha-factor that only relies on the uncertainty in H_s, α_R reflects forecast uncertainties in both H_s and T_p to guide marine operations.

6. Allowable sea states assessment

Allowable sea states are finally assessed through a comparison between the R_{E_WF} (adjusted by the α_R) and the corresponding allowable limits. In the following parts, allowable sea states associated with the blade root radial motion and velocity are shown separately. For the blade root radial motion, the allowable limit is defined as the gap

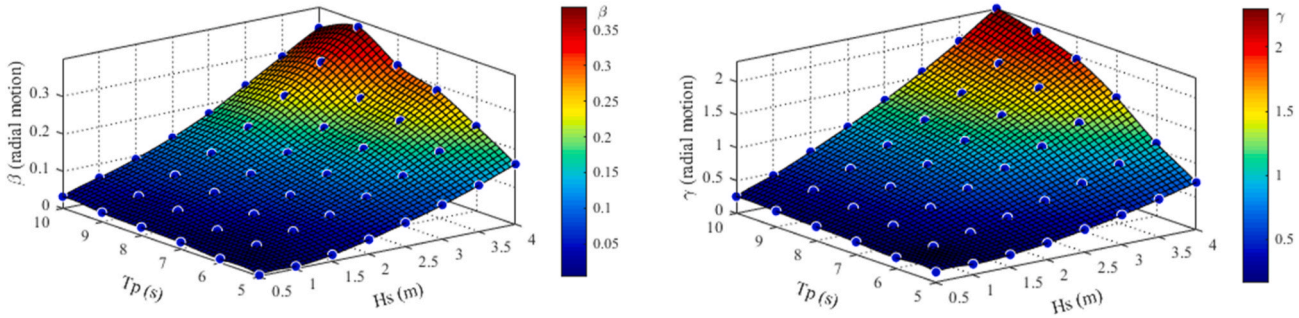

(a) β (b) γ

Fig. 14. Fitting surface of Gumbel parameters as a function of H_s and T_p (blade root radial motion).

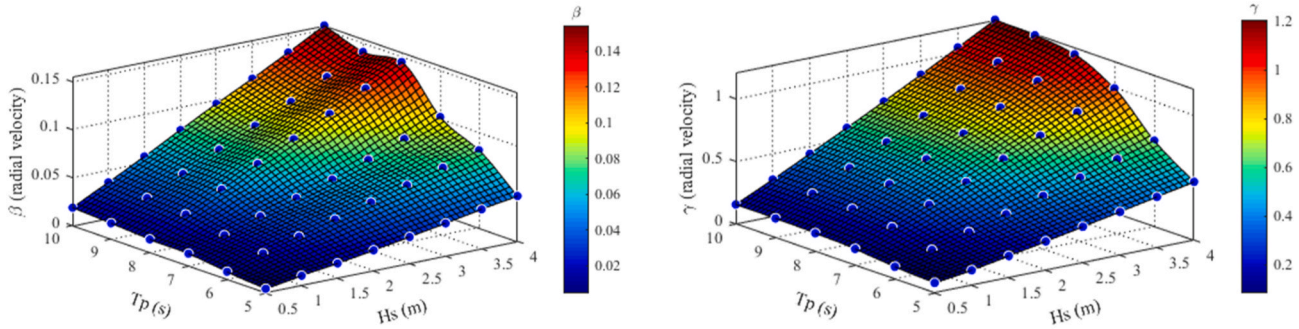

(a) β (b) γ

Fig. 15. Fitting surface of Gumbel parameters as a function of H_s and T_p (blade root radial velocity).

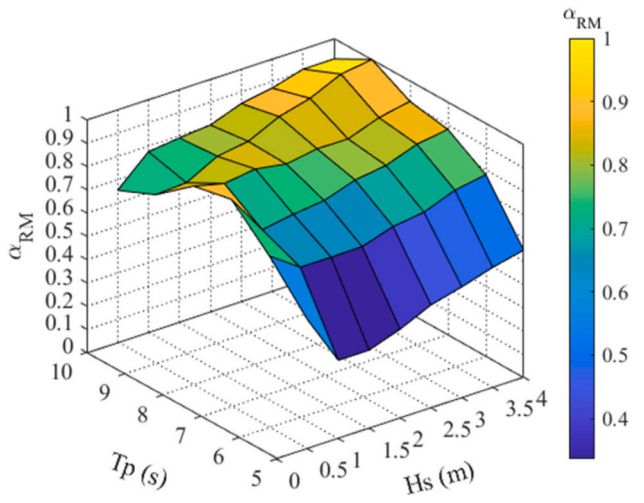

Fig. 16. α_{RM} with a lead time of 3 h.

between the hub radius and blade root radius during the mating phase. Fig. 19 shows a sensitivity study on the allowable limit, in which $0.5R_{root}$, $0.3R_{root}$ and $0.2R_{root}$ are selected as the allowable limit, where R_{root} is the radius of blade root which is 2.69 m. For the blade root radial velocity, the allowable limit is normally related to the plastic bending in the guide pins. A reference velocity (0.7 m/s) proposed by Verma et al. (2019a) is applied in this study as the allowable limit of the blade root radial velocity. Correspondingly, Fig. 20 shows the allowable sea states using the blade root radial velocity as criteria. In Figs. 19 and 20, both the allowable sea states with (dash lines) and without (solid lines) weather forecast uncertainty are presented as functions of H_s and T_p. They represent the maximum allowable sea states, and all sea states below the lines imply that the operation can be safely executed. The dash lines with different colors correspond to weather forecast uncertainties at different lead times. Obviously, once these contour lines are generated, they can be used easily and directly. According to the comparison between weather forecast value of a certain lead time and the corresponding allowable sea states, the decision on whether or not to start the operation can be quickly made.

As displayed in Figs. 19 and 20, the allowable sea state is significantly affected by the sea state forecast uncertainty, since an obvious discrepancy between the solid line and dash lines can be observed. Uncertainty in sea state forecasts decreases the allowable sea state, especially in the range of short T_p. Moreover, the comparison among the dash lines in each figure indicates that the forecast horizon is another important parameter for determining the allowable sea states when the weather forecast uncertainty is taken into account. As expected, the allowable sea states gradually decrease with the forecast lead time T_L increases. This is because when the forecast lead time increases, the weather forecast becomes more uncertain, which reduces the α_R and therefore makes the allowable sea states more conservative. For instance, in Fig. 19 (a), when T_p is 5 s, allowable H_s without forecast uncertainty is about 2 m, while allowable H_s with lead times of 3 and 24 h are about 1.9 m and 1.3 m, respectively. In addition, the importance of the pre-determined allowable limit is also illustrated in Fig. 19. The

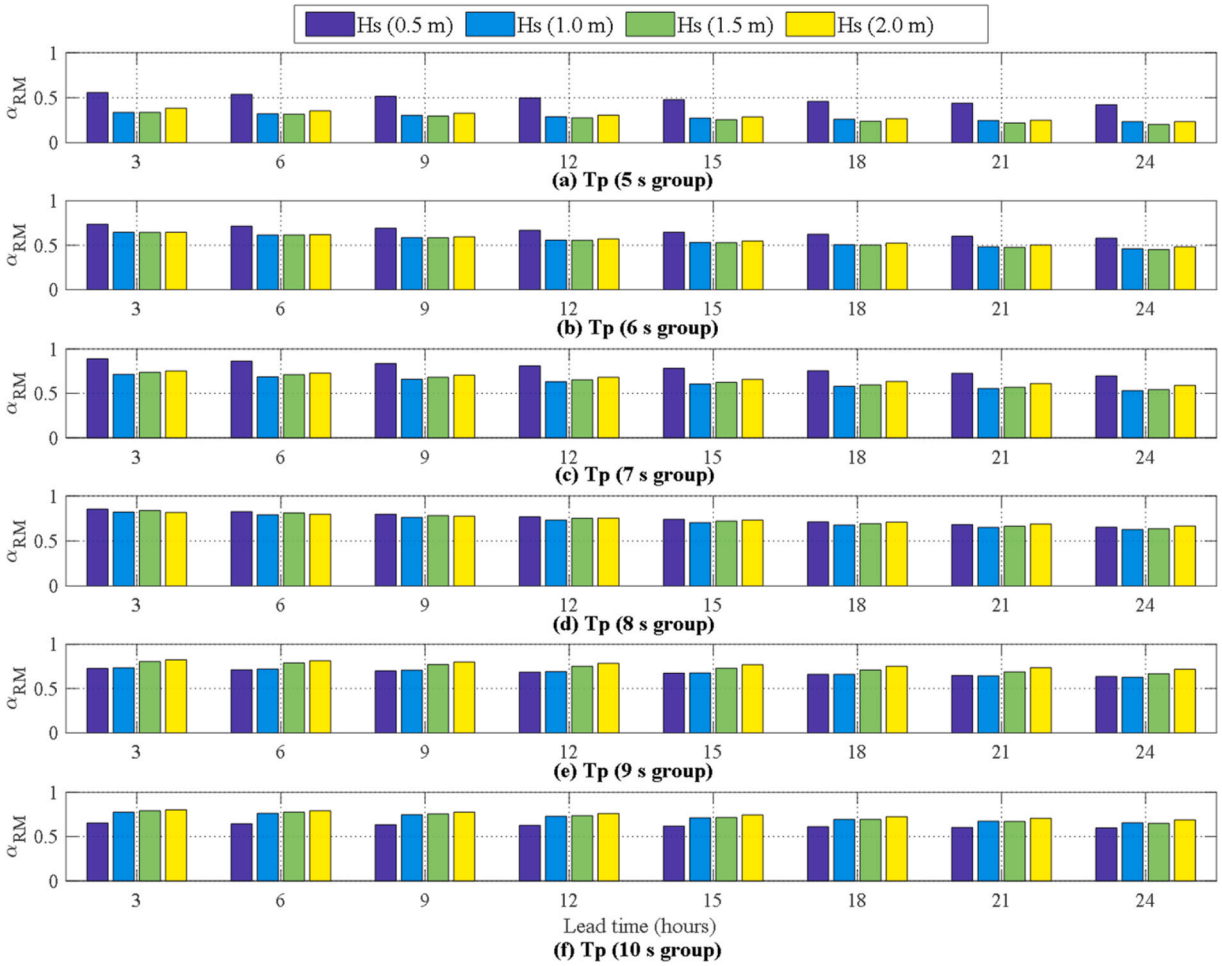

Fig. 17. Variation of α_{RM} with lead times in different H_s groups.

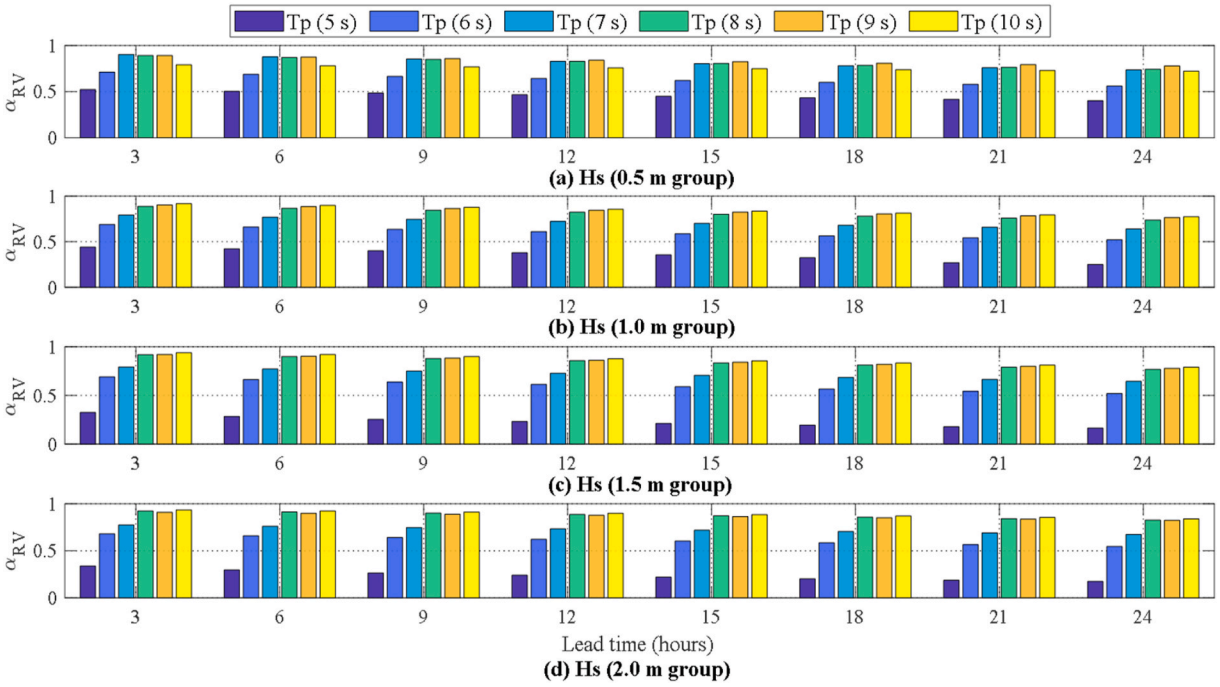

Fig. 18. Variation of α_{RV} with lead times in different T_p groups.

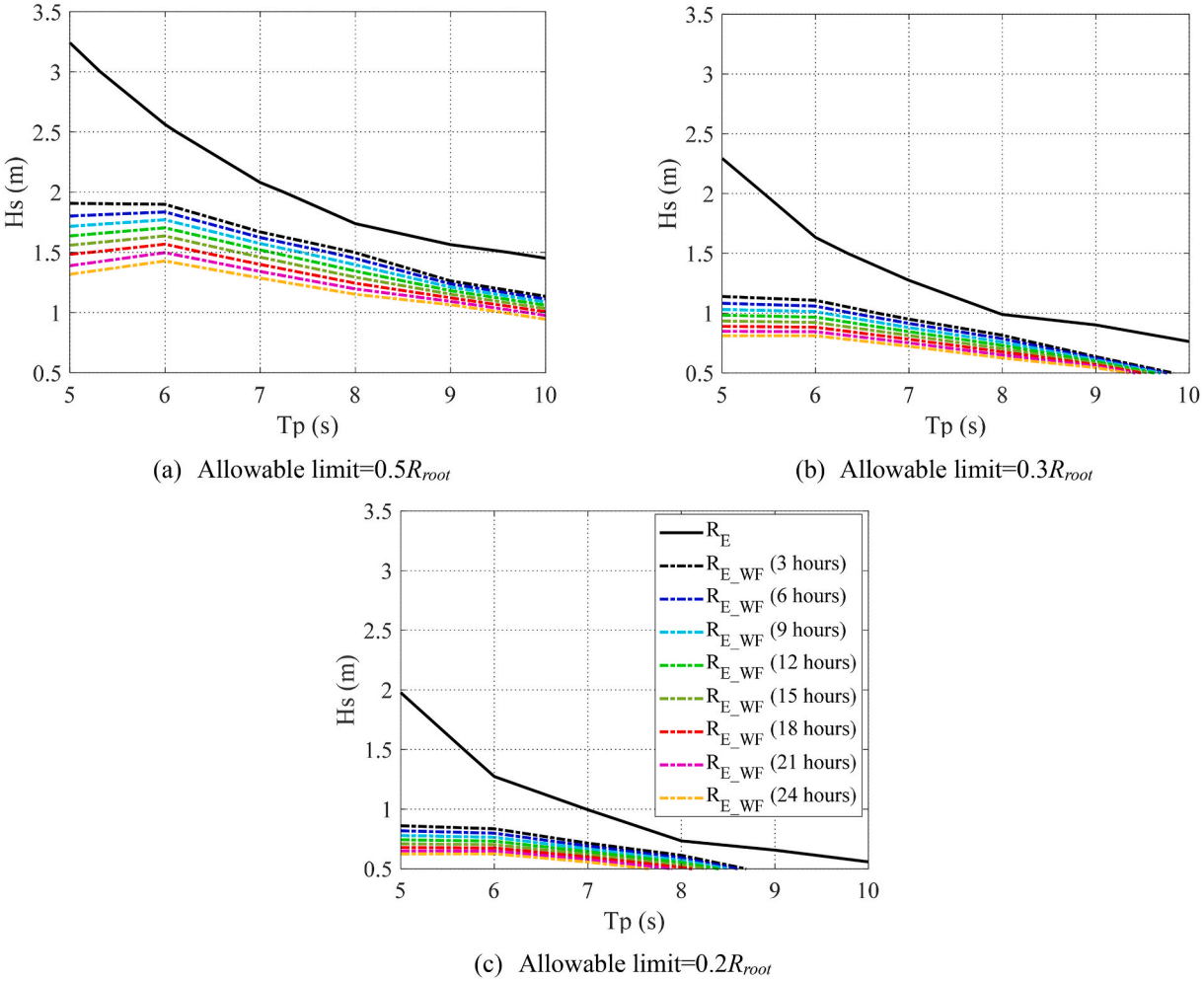

Fig. 19. Allowable sea states of the blade root radial motion.

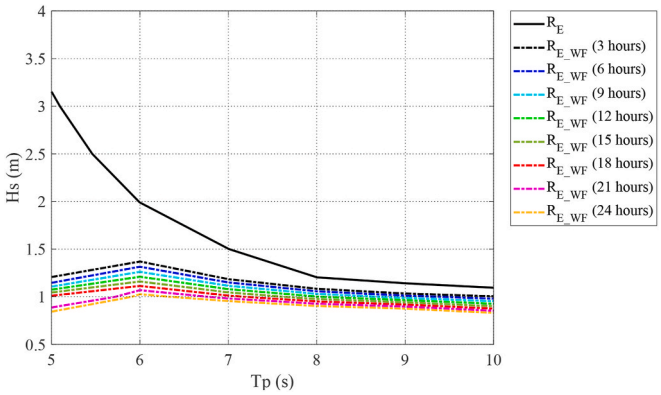

Fig. 20. Allowable sea states of the blade root radial velocity (allowable limit = 0.7 m/s).

comparison among the three examples shows that small allowable limit requires a more accurate operation, and therefore, the allowable sea states will be reduced by high performance requirement.

Furthermore, the workable weather windows for offshore blade installation can be identified by comparing the allowable sea states with weather forecasts. It is important to emphasize that if the operation is controlled by more than one limiting response parameter, identification of workable weather windows is relatively complicated. Regarding the final mating phase, the blade root radial motion and velocity should be considered simultaneously, and the overall weather window should be identified and selected considering the two corresponding windows. This also depends on the pre-determined allowable limits. For instance, if the allowable limit of the blade root radial motion is selected as $0.5R_{root}$ (see Fig. 19 (a)), the allowable sea states related to the blade root radial velocity are lower than those related to the blade root radial motion at every lead time. As a consequence, the overall workable weather window is decided by the blade root radial velocity. In contrast, if the allowable limit of the blade root radial motion is $0.2R_{root}$ (see Fig. 19 (c)), the corresponding weather windows will be shorter than that for the blade root radial velocity. In this case, the weather window for the blade root radial motion decides the overall workable weather windows. However, when the allowable limit of the blade root radial motion is $0.3R_{root}$ (see Fig. 19 (b)), two weather windows should be taken into account simultaneously. Specifically, it is necessary to identify weather windows separately for each limiting parameter, and the overlap part will be the reference for the selection of overall workable weather windows.

7. Conclusions

In this paper, a response-based method for assessing the allowable sea states of offshore single blade installation is developed, with emphasis on both considering weather forecast uncertainty and using time-domain numerical models. It includes the establishment of the response-based alpha-factor α_R to measure the effect of forecast uncertainty in sea states (H_s, T_p) on the system responses, and the assessment of operation allowable sea states.

The general procedure for establishing the α_R in the planning phase based on time-domain modelling and analysis of blade installation, and then assessing corresponding allowable sea states in the execution phase is presented. To establish the α_R, two important analyses should be carried out, namely, the dynamic response analysis of the installation system and the uncertainty quantification of sea state forecasts. Specifically, steady-state time-domain simulations of the final mating phase for blade installation are carried out to assess dynamic responses of the limiting response parameter (i.e., the blade root radial model and velocity). Meanwhile, sea state forecasts are generated and quantified by the pre-defined error factors with respect to the range of sea sates and the forecast lead time. Based on the probabilistic assessment of dynamic responses together with the quantification result of sea state forecasts, the α_R can finally be obtained by a comparison between the characteristic values of the limiting response parameters with and without weather forecast uncertainty. In the execution phase, the established α_R are used to adjust the corresponding characteristic response values to include the effect of sea state forecast uncertainty. The allowable sea states of blade root radial motion and velocity are then assessed separately by comparing the adjusted characteristic values with the corresponding allowable limits. These allowable sea states are able to identify the weather windows through a comparison with the updated sea state forecasts.

Allowable sea states for offshore blade installation using a semi-submersible crane vessel at the North Sea center is assessed. One-day-ahead sea state forecasts generated by the PBML method is utilized in the uncertainty quantification analysis. Besides, a simple uncertainty model is also developed to show how to quantify forecast uncertainty by directly applying commonly used error statistics RMSE and bias. Regarding the time-domain response analysis approach, the effect of statistical uncertainty related to the use of a limited number of simulations to derive the characteristic response values is also investigated and is found small. Quantitative assessment of the dynamic responses shows that the radial motion and velocity of the blade root are sensitive to both H_s and T_p. In addition to the forecast uncertainty of H_s, that of T_p is also critical and needs to be considered during the installation. Compared to the α-factor, the α_R takes sea state forecast uncertainties into account more comprehensive and reflects their effect on the system dynamic response. If the sea state forecast uncertainty is not considered, the allowable sea state may be greatly over-estimated. As the forecast lead time increases, the allowable sea states gradually decrease. Overall, in the execution phase of offshore blade installation by a floating crane vessel, it is necessary to develop the α_R to involve weather forecast uncertainties at different lead times, which can reduce the operational limit reasonably and provide a good reference for the allowable sea state assessment to improve the safety of the installation.

Nevertheless, it should be noted that the variation of the wave direction and wind field are not considered in this study. Besides, only forecast uncertainty in sea states are investigated due to the marginal effects of wind conditions on the installation system. To get more reliably α_R and further assess the allowable sea states with higher accuracy, more comprehensive studies are required in future work. Furthermore, the performance and efficiency of the forecasting method is another key point that determines the practicality of the α_R. More efforts are still needed to further improve the reliability of the α_R by adopting more accurate weather forecasting methods.

CRediT authorship contribution statement

Mengning Wu: Conceptualization, Methodology, Software, Formal analysis, Writing – original draft. **Zhen Gao:** Methodology, Writing – review & editing, Supervision. **Yuna Zhao:** Software, Writing – review & editing.

Declaration of competing interest

The authors declare that they have no known competing financial interests or personal relationships that could have appeared to influence the work reported in this paper.

Acknowledgments

This work was supported by the Centre for Marine Operations in Virtual Environments (MOVE) and Centre for Autonomous Marine Operations and Systems (AMOS), at the Department of Marine Technology, NTNU, Trondheim, Norway. The support is gratefully acknowledged by the authors.

References

Bak, C., Zahle, F., Bitsche, R., Kim, T., Yde, A., Henriksen, L.C., Hansen, M.H., Blasques, J.P.A.A., Gaunaa, M., Natarajan, A., 2013. The DTU 10-MW reference wind turbine. Dan. Wind Power Res. 2013.

Booij, N., Ris, R.C., Holthuijsen, L.H., 1999. A third-generation wave model for coastal regions: 1. Model description and validation. J. Geophys. Res.: Oceans 104 (C4), 7649–7666.

Campos, R., Bernardino, M., Gonçalves, M., Soares, C.G., 2022a. Assessment of metocean forecasts for hurricane lorenzo in the Azores Archipelago. Ocean Eng. 243, 110292.

Campos, R., D'Agostini, A., França, B., Damião, A., Soares, C.G., 2022b. Implementation of a multi-grid operational wave forecast in the South Atlantic Ocean. Ocean Eng. 243, 110173.

Campos, R.M., Alves, J.-H.G., Penny, S.G., Krasnopolsky, V., 2020a. Global assessments of the NCEP Ensemble Forecast System using altimeter data. Ocean Dynam. 70 (3), 405–419.

Campos, R.M., Costa, M.O., Almeida, F., Guedes Soares, C., 2021. Operational wave forecast selection in the Atlantic Ocean using random forests. J. Mar. Sci. Eng. 9 (3), 298.

Campos, R.M., Krasnopolsky, V., Alves, J.-H., Penny, S.G., 2020b. Improving NCEP's global-scale wave ensemble averages using neural networks. Ocean Model. 149, 101617.

Chen, H., 2006. Ensemble prediction of ocean waves at NCEP. In: Proc. 28th Ocean Engineering Conference. Citeseer.

DNV, G., 2011. DNV-OS-H101: Marine Operations. General, Offshore Standard.

Fritsch, F.N., Carlson, R.E., 1980. Monotone piecewise cubic interpolation. SIAM J. Numer. Anal. 17 (2), 238–246.

Group, T.W., 1988. The WAM model—a third generation ocean wave prediction model. J. Phys. Oceanogr. 18 (12), 1775–1810.

Guachamin-Acero, W., Li, L., Gao, Z., Moan, T., 2016. Methodology for assessment of the operational limits and operability of marine operations. Ocean Eng. 125, 308–327.

Harpham, Q., Tozer, N., Cleverley, P., Wyncoll, D., Cresswell, D., 2016. A Bayesian method for improving probabilistic wave forecasts by weighting ensemble members. Environ. Model. Software 84, 482–493.

Hassan, M., Soares, C.G., 2020. Installation of Pre-assembled Offshore Floating Wind Turbine Using a Floating Vessel, Developments in Renewable Energies Offshore. CRC Press, pp. 461–468.

Hoerner, S.F., Borst, H.V., 1975. Fluid-dynamic lift: practical information on aerodynamic and hydrodynamic lift. STIA 76, 32167.

Horner, S., 1965. Fluid Dynamic Drag, Practical Information on Aerodynamic Drag and Hydrodynamic Resistance. Hoerner Fluid Dyn., Midland Park, NJ.

Hudson, B., 2020. Time-domain Simulations of Marine Operations and Their Application to the Offshore Renewable Energy Sector.

IEC, I., 2009. 61400-3, Win. In: d Turbines-Part 3: Design Requirements for Offshore Wind Turbines. International Electrotechnical Commission, Geneva.

JIP, D., 2007. Marine Operation Rules. Technical report. Revised Alpha Factor—Joint Industry Project. DNV, Oslo.

Jonkman, B.J., Buhl Jr., M., 2007. TurbSim User's Guide: Revised February 2007 for Version 1.21. National Renewable Energy Lab.(NREL), Golden, CO (United States).

JR, B., October 4, 2017. Intercomparison of operational wave forecasting systems against buoys: data from ECMWF, MetOffice, FNMOC, MSC, NCEP, MeteoFrance, BoM, SHOM, JMA, KMA, Puerto del Estado, DMI, NZM, METNO, SHN-SM. May 2017 to July 2017, European Centre for Medium-range Weather Forecasts (ECMWF).

Laloyaux, P., de Boisseson, E., Balmaseda, M., Bidlot, J.R., Broennimann, S., Buizza, R., Dalhgren, P., Dee, D., Haimberger, L., Hersbach, H., 2018. CERA-20C: a coupled reanalysis of the Twentieth Century. J. Adv. Model. Earth Syst. 10 (5), 1172–1195.

Leutbecher, M., Palmer, T.N., 2008. Ensemble forecasting. J. Comput. Phys. 227 (7), 3515–3539.

Li, L., Gao, Z., Moan, T., 2015. Joint distribution of environmental condition at five european offshore sites for design of combined wind and wave energy devices. J. Offshore Mech. Arctic Eng. 137 (3).

Li, L., Parra, C., Zhu, X., Ong, M.C., 2020. Splash zone lowering analysis of a large subsea spool piece. Mar. Struct. 70, 102664.

Molteni, F., Buizza, R., Palmer, T.N., Petroliagis, T., 1996. The ECMWF ensemble prediction system: methodology and validation. Q. J. R. Meteorol. Soc. 122 (529), 73–119.

O'Donncha, F., Zhang, Y., Chen, B., James, S.C., 2019. Ensemble model aggregation using a computationally lightweight machine-learning model to forecast ocean waves. J. Mar. Syst. 199, 103206.

Ocean, S., 2017. SIMO-Theory Manual, version 4.10.

Palmer, T.N., 2001. A nonlinear dynamical perspective on model error: a proposal for non-local stochastic-dynamic parametrization in weather and climate prediction models. Q. J. R. Meteorol. Soc. 127 (572), 279–304.

Roh, M., Kim, H.-S., Chang, P.-H., Oh, S.-M., 2021. Numerical simulation of wind wave using ensemble forecast wave model: a case study of typhoon lingling. J. Mar. Sci. Eng. 9 (5), 475.

Saetra, Ø., Bidlot, J.-R., 2004. Potential benefits of using probabilistic forecasts for waves and marine winds based on the ECMWF ensemble prediction system. Weather Forecast. 19 (4), 673–689.

Sintef, O., 2015. SIMA 3.2 User Guide. Technical report.

Sintef, O., 2017. RIFLEX 4.10. 0 Theory Manual. Trondheim, SINTEF Ocean [Online] Available from:[Accessed 5th January 2018].

Smith, I., Lewis, T., Miller, B., Lai, P., Frieze, P., 1996. Limiting motions for jack-ups moving onto location. Mar. Struct. 9 (1), 25–51.

TC88-MT, I., 2005. Iec 61400-3: Wind Turbines–Part 1: Design Requirements, vol. 64. International Electrotechnical Commission, Geneva.

Thomsen, K., 2014. Offshore Wind: a Comprehensive Guide to Successful Offshore Wind Farm Installation. Academic Press.

Tolman, H.L., 1991. A third-generation model for wind waves on slowly varying, unsteady, and inhomogeneous depths and currents. J. Phys. Oceanogr. 21 (6), 782–797.

Veritas, D.N., 2010. Recommended Practice DNV-RP-C205: Environmental Conditions and Environmental loads. DNV, Norway.

Verma, A.S., Jiang, Z., Vedvik, N.P., Gao, Z., Ren, Z., 2019a. Impact assessment of a wind turbine blade root during an offshore mating process. Eng. Struct. 180, 205–222.

Verma, A.S., Vedvik, N.P., Gao, Z., 2017. Numerical assessment of wind turbine blade damage due to contact/impact with tower during installation. In: IOP Conference Series: Materials Science and Engineering. IOP Publishing, 012025.

Verma, A.S., Vedvik, N.P., Gao, Z., 2019b. A comprehensive numerical investigation of the impact behaviour of an offshore wind turbine blade due to impact loads during installation. Ocean Eng. 172, 127–145.

Verma, A.S., Zhao, Y., Gao, Z., Vedvik, N.P., 2019c. Explicit structural response-based methodology for assessment of operational limits for single blade installation for offshore wind turbines. In: Proceedings of the Fourth International Conference in Ocean Engineering (ICOE2018). Springer, pp. 737–750.

Wu, M., Gao, Z., 2021. Methodology for developing a response-based correction factor (alpha-factor) for allowable sea state assessment of marine operations considering weather forecast uncertainty. Mar. Struct. 79, 103050.

Wu, M., Stefanakos, C., Gao, Z., 2020. Multi-step-ahead forecasting of wave conditions based on a physics-based machine learning (PBML) model for marine operations. J. Mar. Sci. Eng. 8 (12), 992.

Zhao, Y., 2019. Numerical Modelling and Dynamic Analysis of Offshore Wind Turbine Blade Installation.

Zhao, Y., Cheng, Z., Gao, Z., Sandvik, P.C., Moan, T., 2019. Numerical study on the feasibility of offshore single blade installation by floating crane vessels. Mar. Struct. 64, 442–462.

Zhao, Y., Cheng, Z., Sandvik, P.C., Gao, Z., Moan, T., 2018a. An integrated dynamic analysis method for simulating installation of single blades for wind turbines. Ocean Eng. 152, 72–88.

Zhao, Y., Cheng, Z., Sandvik, P.C., Gao, Z., Moan, T., Van Buren, E., 2018b. Numerical modeling and analysis of the dynamic motion response of an offshore wind turbine blade during installation by a jack-up crane vessel. Ocean Eng. 165, 353–364.

Zhu, H., Li, L., Ong, M., 2017. Study of Lifting Operation of a Tripod Foundation for Offshore Wind Turbine, IOP Conference Series: Materials Science and Engineering. IOP Publishing, 012012.